curred in the zoo was presumed to have been spread by a single strain, because the infection was limited to primate groups within a particular zone of the zoo at around the same time. The route of transmission of the infection from the isolated group of primates in captivity, including individuals infected with JSK04-Eh-V, to the other groups has not been determined. It is possible that the cysts are the causative agents of JSK04-Eh-V infection, because *E. histolytica* cysts have been reported to be capable of surviving and retaining their infectivity for a month under appropriate wet conditions.[17]

The symptoms of the zoo primates infected with JSK04-Eh-V differed considerably depending on their species; the symptoms in the De Brazza's guenon were relatively mild, while symptoms in the Abyssinian colobus monkey and Geoffroy's spider monkey were severe and fatal. There appear to be species-specific differences among the primates with regard to susceptibility. Although the transmission route was not clear, it is possible that the primates may be carriers and may thus be a source of the parasite. Prior to this study, JSK04-Eh-V infection was thought to have been eradicated, owing to the diligence of the veterinarians and zookeepers working in the zoo, and, fortunately, no zoonotic infection (including amoebiasis) was found among the zookeepers.

YIMDHA-S was designed for the axenic culture of *E. histolytica*, JSK04-Eh-V, and *E. dispar*. This medium is considered to be efficient in comparing biological characteristics of JSK04-Eh-V with *E. histolytica* and *E. dispar*, such as the intensity of in vitro virulence to mammalian tissue culture cell lines,[9] in a single medium under the same culture conditions.

Acknowledgment: A part of this work was supported by a Health Sciences Research Grant-in-Aid for Emerging and Reemerging Infectious Diseases from the Ministry of Health, Labour and Welfare of Japan.

LITERATURE CITED

1. Diamond, L. S., and C. G. Clark. 1993. A redescription of *Entamoeba histolytica* Schaudinn, 1903 (Emended Walker, 1911) separating it from *Entamoeba dispar* Brumpt, 1925. J. Eukaryot. Microbiol. 40(3): 340–344.

2. Diamond, L. S., D. R. Harlow, and C. C. Cunnick. 1978. A new medium for the axenic cultivation of *Entamoeba histolytica* and other *Entamoeba*. Trans. R. Soc. Trop. Med. Hyg. 72(3): 431–432.

3. Evangelopoulos, A., G. Spanakos, E. Patsoula, N. Vakalis, and N. Legakis. 2000. A nested, multiplex, PCR assay for the simultaneous detection and differentiation of *Entamoeba histolytica* and *Entamoeba dispar* in faeces. Ann. Trop. Med. Parasitol. 94: 233–240.

4. Ghosh, S., M. Frisardi, L. Ramirez-Avila, S. Descoteaux, K. Sturm-Ramirez, O. A. Newton-Sanchez, J. I. Santos-Preciado, C. Ganguly, A. Lohia, S. Reed, and J. Samuelson. 2000. Molecular epidemiology of *Entamoeba* spp.: evidence of a bottleneck (demographic sweep) and transcontinental spread of diploid parasites. J. Clin. Microbiol. 38: 3815–3821.

5. Haque, R., I. K. Ali, S. Akther, and W. A. Petri, Jr. 1998. Comparison of PCR, isoenzyme analysis, and antigen detection for diagnosis of *Entamoeba histolytica* infection. J. Clin. Microbiol. 36: 449–452.

6. Kobayashi, S., E. Imai, A. Haghighi, S. A. Khalifa, H. Tachibana, and T. Takeuchi. 2005. Axenic cultivation of *Entamoeba dispar* in newly designed yeast extract-iron-gluconic acid-dihydroxyacetone-serum medium. J. Parasitol. 91: 1–4.

7. Li, E., C. Kunz-Jenkins, and S. L. Stanley, Jr. 1992. Isolation and characterization of genomic clones encoding a serine-rich *Entamoeba histolytica* protein. Mol. Biochem. Parasitol. 50(2): 355–357.

8. Petri, W. A., Jr., R. D. Smith, P. H. Schlesinger, C. F. Murphy, and J. I. Ravdin. 1987. Isolation of the galactose-binding lectin that mediates the in vitro adherence of *Entamoeba histolytica*. J. Clin. Invest. 80: 1238–1244.

9. Ravdin, J. I., and R. L. Guerrant. 1982. Separation of adherence, cytolytic, and phagocytic events in the cytopathogenic mechanisms of *Entamoeba histolytica*. Arch. Invest. Med. 13: 123–128.

10. Ritchie, L. S. 1948. An ether sedimentation technique for routine stool examinations. Bull. U. S. Army Med. Dept. 8: 326.

11. Suzuki, J., S. Kobayashi, R. Murata, Y. Yanagawa, and T. Takeuchi. 2007. Profile of a pathogenic *Entamoeba histolytica*-like variant with variations in the nucleotide sequence of the small subunit ribosomal RNA isolated from a primate (De Brazza's Guenon). J. Zoo Wildl. Med. 38(3): 471–474.

12. Tachibana, H., X. J. Cheng, S. Kobayashi, N. Matsubayashi, S. Gotoh, and K. Matsubayashi. 2001. High prevalence of infection with *Entamoeba dispar*, but not *E. histolytica*, in captive macaques. Parasitol. Res. 87: 114–117.

13. Tachibana, H., T. Yanagi, K. Pandey, X. J. Cheng, S. Kobayashi, J. B. Sherchand, and H. Kanbara. 2007. An *Entamoeba* sp. strain isolated from rhesus monkey is virulent but genetically different from *Entamoeba histolytica*. Mol. Biochem. Parasitol. 153(2): 107–114.

14. Takano, J., T. Narita, H. Tachibana, T. Shimizu, H. Komatsubara, K. Terao, and K. Fujimoto. 2005. *Entamoeba histolytica* and *Entamoeba dispar* infections in cynomolgus monkeys imported into Japan for research. Parasitol. Res. 97: 255–257.

15. Takano, J., T. Narita, H. Tachibana, K. Terao, and K. Fujimoto. 2007. Comparison of *Entamoeba histolytica* DNA isolated from a cynomolgus monkey with human isolates. Parasitol. Res. 101(3): 539–546.

16. Verweij, J. J., A. M. Polderman, and C. G. Clark. 2001. Genetic variation among human isolates of uninu-

cleated cyst-producing *Entamoeba* species. J. Clin. Microbiol. 39(4): 1644–1646.

17. Walsh, J. A. 1988. Transmission of *Entamoeba histolytica* infection. *In:* Amebiasis. Wiley Medical, John Wiley and Sons, Inc., New York, New York. Pp. 106–126.

18. World Health Organization. 1995. The World Health Report 1995: Bridging the Gaps, vol. 16. World Health Organization, Geneva, Switzerland. Pp. 28–29.

19. World Health Organization. 1997. Amoebiasis. W. H. O. Wkly. Epidemiol. Rec. 72: 97–100.

20. Zaki, M., and C. G. Clark. 2001. Isolation and characterization of polymorphic DNA from *Entamoeba histolytica*. J. Clin. Microbiol. 39(3): 897–905.

Received for publication 12 December 2007

nature medicine

Interferon-g is a therapeutic target molecule for prevention of postoperative adhesion formation

Hisashi Kosaka[1,5], Tomohiro Yoshimoto[2,3,5], Takayuki Yoshimoto[4], Jiro Fujimoto[1] & Kenji Nakanishi[2,3]

Intestinal adhesions are bands of fibrous tissue that connect the loops of the intestine to each other, to other abdominal organs or to the abdominal wall[1–3]. Fibrous tissue formation is regulated by the balance between plasminogen activator inhibitor type 1 (PAI-1) and tissue-type plasminogen activator (tPA), which reciprocally regulate fibrin deposition. Several components of the inflammatory system, including cytokines[4], chemokines, cell adhesion molecules and neuropeptide substance P, have been reported to participate in adhesion formation[4–7]. We have used cecal cauterization to develop a unique experimental mouse model of intestinal adhesion. Mice developed severe intestinal adhesion after this treatment. Adhesion development depended upon the interferon-c (IFN-c) and signal transducer and activator of transcription-1 (STAT1) system. Natural killer T (NKT) cell–deficient mice developed adhesion poorly, whereas they developed severe adhesion after reconstitution with NKT cells from wild-type mice, suggesting that NKT cell IFN-c production is indispensable for adhesion formation. This response does not depend on STAT4, STAT6, interleukin-12 (IL-12), IL-18, tumor necrosis factor-a, Toll-like receptor 4 or myeloid differentiation factor-88–mediated signals. Wild-type mice increased the ratio of PAI-1 to tPA after cecal cauterization, whereas $Ifng^{-/-}$ or $Stat1^{-/-}$ mice did not, suggesting that IFN-c has a crucial role in the differential regulation of PAI-1 and tPA. Additionally, hepatocyte growth factor, a potent mitogenic factor for hepatocytes[8,9], strongly inhibited intestinal adhesion by diminishing IFN-c production, providing a potential new way to prevent postoperative adhesions.

Abdominal adhesion formation occurs in 67–93% of abdominal surgeries[10–13]. Adhesion also develops after abdominal bacterial infections, such as peritonitis[14]. A recent study has indicated that T helper type 1 (T_H1) cells are essential for the development of adhesion in a mouse model of intra-abdominal sepsis[15]. Nevertheless, only a limited number of studies have investigated the molecular process involved in intestinal adhesions. In addition, there are no appropriate treatments for or ways to prevent intestinal adhesions. Here we have established a unique experimental mouse model for elucidating the molecular mechanism underlying organ adhesions.

We induced intestinal adhesion by cecal cauterization using the coagulation mode of bipolar forceps. A time-course experiment revealed that this treatment induced progressive inflammatory and fibrotic changes (Supplementary Fig. 1a online). Adhesions strongly connected the cecum to the large bowel, the abdominal wall or both at day 7. Wild-type mice formed thick adhesion with plantar attachment (which we gave a score of 4) or developed very thick vascularized adhesion (score 5; Supplementary Fig. 1b). This fibrotic structure was firm and difficult to remove from the involved organs. In contrast, mice that underwent control laparotomy without cecal cauterization had no adhesion (score 0; Supplementary Fig. 1b).

To understand the immunological mechanism underlying cauterization-induced intestinal adhesion, we examined mice depleted of $CD4^+$T cells for their capacity to develop adhesion (Fig. 1). These mice had significantly reduced adhesion (score 0 or 1) and fibrotic changes in their ceca, compared with control mice (score 5) ($P < 0.0001$; Fig. 1a,c), suggesting that $CD4^+$T cells are essential in adhesion formation.

Because $CD4^+$ T cells consist of conventional $NK1.1^-CD4^+$ T cells and NKT cells expressing ab T cell receptor with invariant Val14–Jal8 (refs. 16–18), we examined which type of $CD4^+$ T cells contributed to this adhesion formation. Thus, we surgically treated NKT cell–deficient mice[19] by cauterizing isolated ceca and examined their intestinal adhesion formation. These mice developed lower grade (score 1 or 2; $P < 0.0001$) intestinal adhesion and weak fibrotic change (Fig. 1b,c). However, when they were reconstituted with unfractionated $CD4^+$ T cells from wild-type mice, but not from $Ifng^{-/-}$ mice, they gained the capacity to develop severe intestinal adhesion and severe fibrotic changes (Fig. 1b,c). Thus, unlike in a previous mouse model of surgical adhesion formation in which T_H1 cells were essential[15], in our adhesion model NKT cells contributed to intestinal adhesion formation by producing IFN-g.

In general, cytokine messenger RNAs, including IFN-g mRNA, are undetectable in the cecum. However, surgical treatment induced cecum IFN-g mRNA expression, which peaked at 3 h and declined gradually, suggesting immediate IFN-g production by NKT cells

[1]Department of Surgery and [2]Department of Immunology and Medical Zoology, Hyogo College of Medicine, 1-1, Mukogawa, Nishinomiya, Hyogo 663-8501, Japan. [3]Core Research for Evolutional Science and Technology, Japan Science and Technology Corporation, 4-1-8, Honmachi, Kawaguchi, Saitama 332-0012, Japan. [4]Intractable Immune System Disease Research Center, Tokyo Medical University, 6-1-1, Shinjuku, Shinjuku-ku, Tokyo 160-8402, Japan. [5]These authors contributed equally to this work. Correspondence should be addressed to K.N. (nakaken@hyo-med.ac.jp).

Received 13 September 2007; accepted 4 February 2008; published online 16 March 2008; doi:10.1038/nm1733

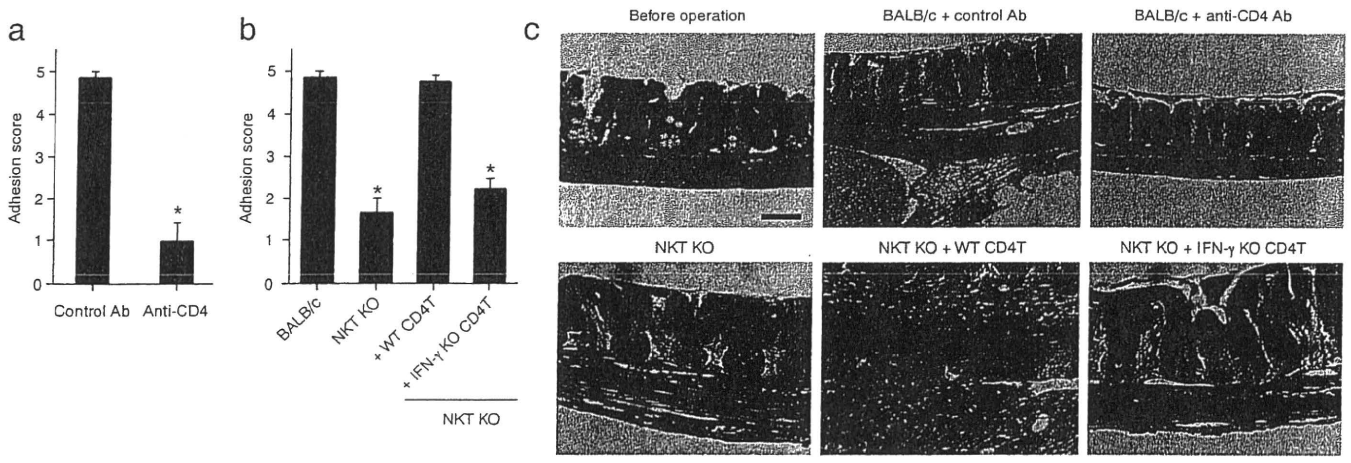

Figure 1 NKT cells are the main contributors to postsurgical adhesion formation. (a,b) BALB/c mice or BALB/c mice depleted of $CD4^+$ T cells by treatment with antibody to CD4, anti-CD4 (a) or NKT cell-deficient (NKT KO) mice or NKT KO mice reconstituted with splenic $CD4^+$ T cells (1.0 10^7 cells per mouse) from wild-type (WT CD4T) or $Ifng^{-/-}$ (IFN-g KO) mice (b) as described in the Methods underwent cecal cauterization surgery. Seven days after operation, mice were killed and examined for adhesion formation. Results are geometric means ± s.e.m. of eight mice per group and are representative of more than three independent experiments. *P o 0.0001 as compared to BALB/c control groups. (c) Seven days after cecal cauterization surgery, each group of mice (as described in a and b) were killed and the isolated ceca were stained with Sirius red. Representative results from eight to ten mice per group are shown. Scale bar, 50 mm.

(Fig. 2a). NKT cell–deficient mice had lower expression of IFN-g mRNA in their ceca (Fig. 2b), further substantiating this possibility. We next examined the capacity of $Ifng^{-/-}$ mice or $Stat1^{-/-}$ mice, which lack molecules required for intracellular signaling of IFN-g, IFN-a and IFN-b (ref. 20), to develop abdominal adhesion (Fig. 2c,d). Both types of mice did not develop abdominal adhesion. However, only $Ifng^{-/-}$ mice gained the capacity to develop intestinal adhesion after administration of IFN-g (Fig. 2c). Next, we examined whether surgical adhesion formation rapidly induced accumulation of NKT cells in the cecal wall. We found a marked and rapid increase in the number of

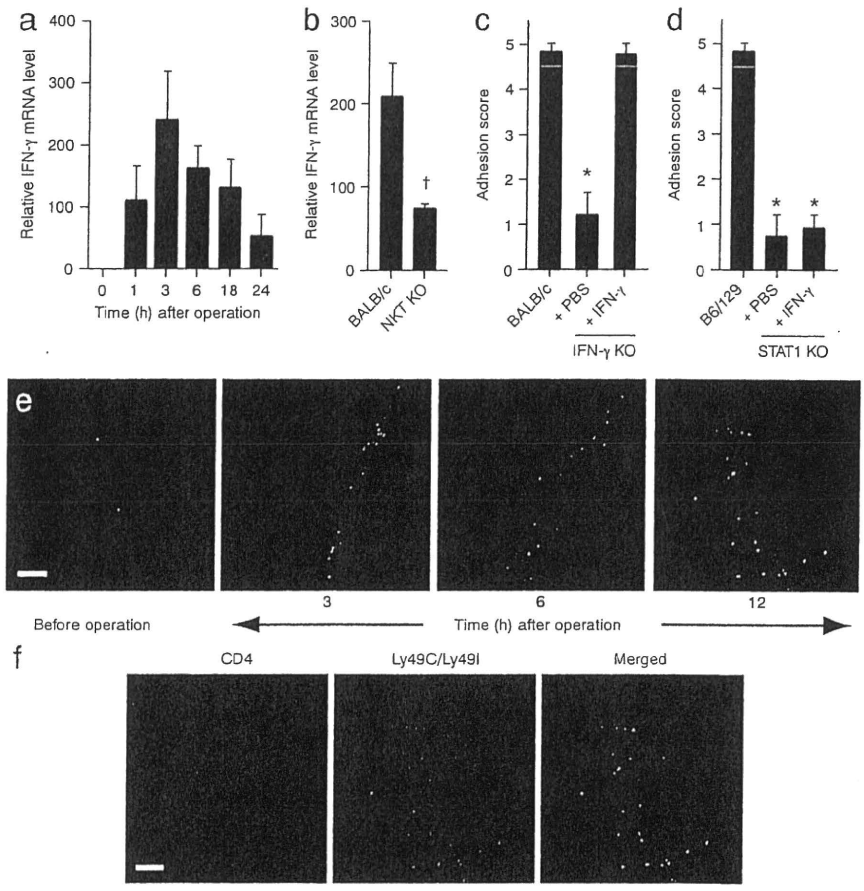

Figure 2 Rapid IFN-g production by NKT cells is causative in postsurgical adhesion formation. (a) Relative IFN-g mRNA expression in isolated cecum from BALB/c mice that had undergone cecal cauterization surgery as determined by real-time PCR. Cecum was isolated before and 1, 3, 6, 18 and 24 h after operation. (b) Relative IFN-g mRNA expression in isolated cecum from BALB/c and NKT KO mice 3 h after cecal cauterization surgery as determined by real-time PCR. Results are geometric means ± s.e.m. of five to eight mice per group and are representative of two independent experiments. wP o 0.05 as compared to control wild-type mice. (c,d) BALB/c mice, IFN-g KO mice (c) and $Stat1^{-/-}$ mice (STAT1 KO; d) injected with PBS or IFN-g by osmotic pumps as described in the Methods underwent cecal cauterization surgery. Seven days after operation, mice were killed and examined for adhesion formation. Results are geometric means ± s.e.m. of five mice per group and are representative of three independent experiments. *P o 0.0001 as compared to control wild-type mice. (e,f) After cecal cauterization, mice were killed and their ceca were taken and frozen at the indicated times (e) and at 12h (f). Frozen sections were fixed and incubated with antibodies to mouse Ly49C/Ly49I and CD4 and then examined by confocal microscopy. CD4, red; Ly49C/Ly49I, green; colocalization, yellow (Merged). Scale bar, 50 mm.

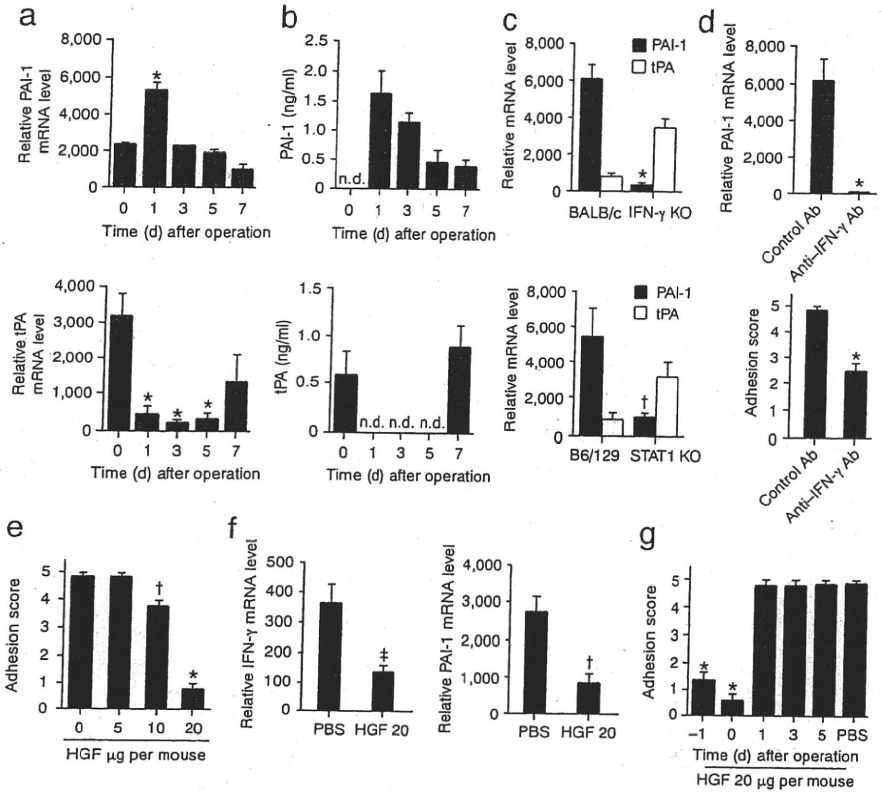

Figure 3 HGF inhibits IFN-g–STAT1–dependent PAI-1 induction and postsurgical adhesion formation. (a–g) BALB/c mice underwent cecal cauterization surgery. The relative mRNA expression of PAI-1 (a,c,d,f) and tPA (a,c) in isolated cecum, PAI-1 and tPA levels in the plasma (b), and adhesion score (d,e,g) were measured (see Methods). (a,b) Ceca and plasma were taken at the indicated days after operation. (c) Ceca were taken 1 d after operation. Results are geometric means ± s.e.m. of five mice per group and are representative of three independent experiments. *P o 0.005 as compared to non-operated control group (a). n.d., not detected (b). *P o 0.0001 and wP o 0.02 as compared to control mice group, respectively (c). (d) Ceca (top) were taken from BALB/c mice injected with IFN-g–specific or control antibodies 2 d before and subsequently treated with cecal cauterization 1 d before. Adhesion formation (bottom) at 7 d after operation was examined. Results are representative of two independent experiments. *P o 0.002 as compared to control groups. (e–g) BALB/c mice were injected with HGF (0–20 mg per mouse) 1 d before cecal cauterization (e,f) or on the days indicated (g). Adhesion formation (bottom) was examined at 7 d after operation (e,g). Three hours and 1 d after operation, the relative IFN-g and PAI-1 mRNA expression in isolated cecum was determined (f). Representative of three independent experiments. *P o 0.0001, wP o 0.005 and zP o 0.02 as compared to control PBS-injected mice.

Ly49$^+$CD4$^+$ T cells (NKT cells)[21] at 3 h after operation (Fig. 2e,f), further substantiating the idea that NKT cells are responsible for rapid IFN-g production after surgical treatment.

Postsurgical adhesion formation in an intra-abdominal septic model was reported to be dependent on the action of CD4$^+$ T_H1 cells[15]. Therefore, we examined whether the T_H1 response or the lipopolysaccharide (LPS) or tumor necrosis factor-a (TNF-a) responses can affect the development of cauterization-induced intestinal adhesion. We have summarized the results in Supplementary Table 1 online. Stat4$^{-/-}$ (ref. 22), Stat6$^{-/-}$ (ref. 23), Il12p40$^{-/-}$ and Il18$^{-/-}$ mice normally developed postsurgical abdominal adhesion. Furthermore, C3H/HeJ mice, which have a point mutation in the gene encoding Toll-like receptor 4 (TLR4), Myd88$^{-/-}$ mice, which lack an adaptor protein for TLRs, and Tnfa$^{-/-}$ mice also normally developed abdominal adhesion (Supplementary Table 1). Therefore, our adhesion model is non–LPS-induced, and T_H1 cells, T_H2 cells, TNF-a or TLR-MyD88–induced signals are not involved. Additionally, this surgical treatment induced the expression of mRNAs for IL-1b, IL-6, IL-17, TNF-a and TGF-b (Supplementary Fig. 2 online).

The proinflammatory neuropeptide substance P can initiate a wide range of adhesiogenic effects[24]. Therefore, Tac1$^{-/-}$ mice, lacking tachykinins, including substance P, neurokinin A, neuropeptide K and neuropeptide g (ref. 25), were tested in their capacity to develop intestinal adhesion. They had a significantly reduced adhesion score (P o 0.001; Supplementary Fig. 3a online) and reduced IFN-g mRNA expression in their ceca (Supplementary Fig. 3b). Furthermore, CD4$^+$ T cells from wild-type mice, but not from NKT cell–deficient mice, produced IFN-g in response to substance P and increased further IFN-g production when additionally stimulated with neurokinin A and neuropeptide K (Supplementary Fig. 3c). These results strongly suggest that tachykinins induce NKT cell IFN-g production.

Because fibrinolysis is regulated by PAI-1 and tPA activity[1,26], we examined whether the ratio of these molecules is regulated by surgical treatment via IFN-g–dependent STAT1 activation. Wild-type mice had increased expression of PAI-1 and decreased expression of tPA, both in their ceca (at the mRNA level) and in their plasma (at the protein level) at day 1 (Fig. 3a,b), whereas Ifng$^{-/-}$ or Stat1$^{-/-}$ mice did not (Fig. 3c), suggesting reciprocal regulation of PAI-1 and tPA activity by IFN-g. Furthermore, wild-type mice pretreated with a single injection of IFN-g–specific antibody (2 mg per mouse) one day before cecal cauterization did not show an increase in PAI-1 mRNA and had significantly less intestinal adhesion (score 2) (P o 0.002; Fig. 3d). Thus, IFN-g is a causative factor in postsurgical adhesion formation.

We have previously reported that hepatocyte growth factor (HGF) treatment strongly suppresses IFN-g mRNA expression in the small intestines of mice with acute graft-versus-host disease[27]. Thus, we injected recombinant HGF protein (5, 10 or 20 mg per mouse) subcutaneously 1 d before operation to examine its preventive effects on adhesion formation. A single injection of HGF (20 mg per mouse) significantly reduced intestinal adhesion (score 0 or 1; Fig. 3e). Furthermore, HGF treatment suppressed mRNAs for IFN-g and PAI-1, suggesting that HGF inhibits PAI-1 via inhibition of IFN-g production (Fig. 3f). HGF injection immediately after operation was proven to be most effective (Fig. 3g).

We have developed a new experimental intestinal adhesion model. We can use bipolar forceps, which we routinely use in human surgery, to induce intestinal adhesion mimicking human intestinal adhesion. We can control the duration and intensity of cauterization by changing the mode, allowing us to treat the mice with identical invasive maneuvers in terms of quantity and quality. The procedure is simple and very straightforward, and the obtained results are very reproducible.

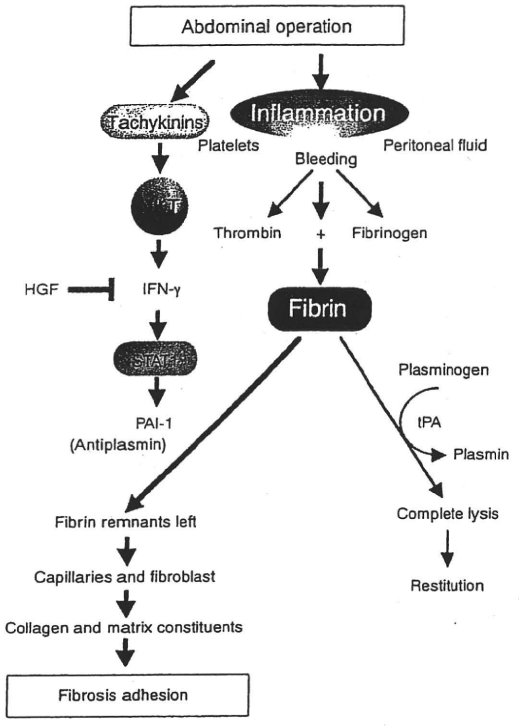

Figure 4 Causative role of NKT cell IFN-g production in induction of postsurgical adhesion formation. The balance between fibrin deposition and fibrin degradation regulates fibrous tissue formation when adhesion formation is experimentally decreased or increased by inhibition of PAI-1 or tPA, respectively. After abdominal operation, NKT cell–derived IFN-g increases the ratio of PAI-1 to tPA by activation of a STAT1-dependent pathway, leading to intestinal adhesion. A single injection of HGF protein completely inhibits intestinal adhesions by downregulation of IFN-g–dependent PAI-1 induction, providing a new potential therapeutic for the prevention of postoperative adhesions.

Other researchers have established the cecal abrasion model, the development of which depends on an IL-12–STAT4–T_H1 system[15]. In contrast, as we report here, cecal cauterization induces intestinal adhesion in an IFN-g–STAT1–NKT cell–dependent manner. In Supplementary Table 2 online, we show the features of our cauterization method and the cecal abrasion method[15]. Our adhesion model is clearly non-T_H1 and non–LPS-induced.

Our present results strongly indicate that induction of abdominal adhesion is principally dependent on endogenous IFN-g (Fig. 1b,c). NKT cells rapidly accumulate in the cecum after cauterization and express IFN-g mRNA at 3 h after treatment (Fig. 2a,e). Furthermore, $Tac1^{-/-}$ mice lacking tachykinins have a lower adhesion score and lower IFN-g mRNA levels (Supplementary Fig. 3), suggesting that tachykinins, including substance P, neurokinin A and neuropeptide K, induce NKT cell IFN-g production in vivo $CD4^+$ T cells from wild-type mice, but not from NKT cell–deficient mice, produce IFN-g in response to substance P, neurokinin A and neuropeptide K (Supplementary Fig. 3c).

Fibrin is important for blood clotting. If there is insufficient fibrinolytic activity, organization of the fibrin matrix and cellular and vascular ingrowths ensue, leading to fibrous bands between organs (Fig. 4)[1–3]. Here, we demonstrate that IFN-g is important for induction of PAI-1, because both $Ifng^{-/-}$ and $Stat1^{-/-}$ mice did not increase expression of PAI-1 mRNA (Fig. 3c). Thus, IFN-g is very important for induction of PAI-1 mRNA, intestinal adhesion formation and blood clotting.

Finally, we demonstrate that HGF strongly prevents intestinal adhesion by inhibiting IFN-g and PAI-1 mRNA expression in the cecum (Fig. 3f). A single injection of IFN-g–specific antibody 1 d before operation effectively inhibits abdominal adhesion (Fig. 3d). Thus, inhibition of immediate IFN-g production after surgical treatment is crucial. Although HGF has many healing effects on the gastrointestinal tract[28], our present data strongly suggest that HGF inhibits intestinal adhesion principally by suppressing rapid IFN-g production after surgical treatment. Additionally, though, the possibility of HGF-associated carcinogenicity has not been completely excluded[28]. But because of the single injection of HGF and its short half-life in the human body, HGF injection seems to be safer than HGF gene therapy, in which HGF is constitutively expressed within a limited area. Recombinant human HGF is already available for people with fatal liver disease; the results presented here strongly indicate that HGF treatment can be a new strategy for prevention of postsurgical adhesion formation.

IFN-g is a very crucial cytokine for host defense. Therefore, careful co-administration of antibiotics might be important during modulation of IFN-g by our approach. HGF treatment seems to be a promising way for preventing adhesion without affecting anastomoses of cut ends of bowel, because this treatment shows healing effects on the gastrointestinal tract. Of course, extensive basic studies are needed to estimate the translational potential of HGF treatment for the prevention of intestinal adhesion formation in human cases.

METHODS

Mice. We purchased BALB/c, C57BL/6 (B6), B6 $Tac1^{-/-}$, BALB/c $Stat6^{-/-}$, C3H/HeN and C3H/HeJ mice from Jackson Laboratory. We bred BALB/c NKT cell–deficient, BALB/c $Ifng^{-/-}$, B6 $Il12p40^{-/-}$, B6 $Il18^{-/-}$, B6 $Myd88^{-/-}$, B6 $Tnfa^{-/-}$ mice under specific pathogen–free conditions at the animal facilities of Hyogo College of Medicine. We bred BALB/c $Stat4^{-/-}$ and 129/Sv $Stat1^{-/-}$ mice under specific pathogen–free conditions in the animal facilities at Tokyo Medical University. All animal experiments were performed in accordance with the guidelines of the Institutional Animal Care Committee, Hyogo College of Medicine and Tokyo Medical University.

Mouse model of surgical adhesion formation. We anesthetized mice with 0.15 ml (20% vol/vol) diluted pentobarbital sodium solution (10 mg/ml). We made an anterior midline incision through the abdominal wall and peritoneum. We isolated the cecum and cauterized it using the coagulation mode of bipolar forceps (MERA; 30 W, 500 kHz, 150 O) for one second. We closed the incision in two layers with silk sutures. Daily histological examination revealed that this surgical treatment did not induce penetration of the intestinal wall, suggesting that the burned site did not induce an influx of bacteria from lumen into peritoneal cavity. We killed the mice 7 d later, when they were examined by an observer blinded to the identity of the experimental groups. Each mouse was evaluated according to the following standard scoring system, which has been widely used in this field[15,29,30]: score 0, no adhesion; score 1, one thin filmy adhesion; score 2, more than one thin adhesion; score 3, thick adhesion with focal point; score 4, thick adhesion with plantar attachment or more than one thick adhesion with focal point; and score 5, very thick vascularized adhesion or more than one plantar adhesion.

Reagents. We purchased recombinant mouse IFN-g and HGF from Genetics Institute and Peprotech, respectively.

In vivo treatment of mice. For adoptive $CD4^+$ T cell transfer experiments, we purified splenic $CD4^+$ T cells from wild-type or $Ifng^{-/-}$ mice with MicroBeads (antibody to mouse CD4; clone RM4-5, Miltenyi Biotec). We transferred $CD4^+$ T cells to NKT cell–deficient mice (1.0 10^7 cells per mouse) via the tail vein route 7 d before surgery. For treatment with IFN-g, we subcutaneously infused osmotic pumps (DURECT) filled with IFN-g (100 mg) in 100 ml PBS into mice

2 d before surgery. The pumping rate of an osmotic pump was 0.5 ml/h continuously, and the duration was 7 d. We subcutaneously injected mice with HGF (0, 5, 10 or 20 mg per mouse) in 200 ml of PBS on the days indicated in Figure 3g before or after surgery. The detailed protocols of antibody treatment to deplete $CD4^+$ T cells and IFN-g are described in the Supplementary Methods online.

Histology. We fixed tissues in 10% buffered formalin, embedded them in paraffin, cut them into 3-mm sections and stained them with H&E or picric acid and Sirius red.

Quantitative reverse transcription PCR. We extracted total RNA from the cecum with the RNeasy Plus Mini Kit (QIAGEN) and synthesized the cDNA using SuperScript III RNase H^- Reverse Transcriptase (Invitrogen). We quantified the expression of the gene with TaqMan Gene Expression Assays (Applied Biosystems). We expressed the results as relative expression standardized with the expression of the gene encoding eukaryotic 18S ribosomal RNA. Specific primers used for quantitative RT-PCR are described in the Supplementary Methods.

Enzyme-linked immunosorbent assay. We measured the abundance of PAI-1 and tPA in plasma with a mouse PAI-1 ELISA kit (Innovative Research) and mouse tPA ELISA kit (Oxford Biomedical Research), respectively.

Statistical analyses. Data are given as means ± s.e.m. We made statistical comparisons between two experimental groups by Student's paired t-test performed with GraphPad Instat Software. We considered a P value o0.05 as significantly different.

Note: Supplementary information is available on the Nature Medicine website.

ACKNOWLEDGMENTS

This study was supported by a Grant-in-Aid for Scientific Research on Priority Areas and a Hitech Research Center grant from the Ministry of Education, Culture, Sports, Science and Technology of Japan and a Grant-in-Aid for Scientific Research (B; No. 19390342) from the Japan Society for Promotion of Science.

AUTHOR CONTRIBUTIONS

Tomohiro Yoshimoto and K.N. formulated the hypothesis and initiated and organized the study; H.K. and Tomohiro Yoshimoto performed the main experimental work and analyzed the data; Takayuki Yoshimoto helped with some experimental procedures; Tomohiro Yoshimoto and K.N. oversaw the experiments, analyzed the data and provided the main funding for the research; J.F. contributed to data discussion; Tomohiro Yoshimoto drafted the manuscript and K.N. prepared the final manuscript.

Published online at http://www.nature.com/naturemedicine
Reprints and permissions information is available online at http://npg.nature.com/reprintsandpermissions

1. Holmdahl, L. The role of fibrinolysis in adhesion formation. Eur. J. Surg. 163 (Suppl. 577), 24–31 (1997).
2. Raftery, A.T. Regeneration of peritoneum: a fibrinolytic study. J. Anat. 129, 659–664 (1979).
3. Sulaiman, H., Dawson, L., Laurent, G.J., Bellingan, G.J. & Herrick, S.E. Role of plasminogen activators in peritoneal adhesion formation. Biochem. Soc. Trans. 30, 126–131 (2002).
4. Holmdahl, L. & Ivarsson, M.L. The role of cytokines, coagulation, and fibrinolysis in peritoneal tissue repair. Eur. J. Surg. 165, 1012–1109 (1999).
5. Fanciullacci, M., Fedi, S., Alessandri, M. & Pietrini, U. Substance P–induced fibrinolysis in the forearm of healthy humans. Experientia 49, 242–244 (1993).
6. Reed, K.L. et al. Neurokinin-1 receptor and substance P messenger RNA levels increase during intraabdominal adhesion formation. J. Surg. Res. 108, 165–172 (2002).
7. Reed, K.L. et al. A neurokinin 1 receptor antagonist decreases postoperative peritoneal adhesion formation and increases peritoneal fibrinolytic activity. Proc. Natl. Acad. Sci. USA 101, 9115–9120 (2004).
8. Miyazawa, K. et al. Molecular cloning and sequence analysis of cDNA for human hepatocyte growth factor. Biochem. Biophys. Res. Commun. 163, 967–973 (1989).
9. Nakamura, T. et al. Molecular cloning and expression of human hepatocyte growth factor. Nature 342, 440–443 (1989).
10. Ellis, H. The clinical significance of adhesions: focus on intestinal obstruction. Eur. J. Surg. 163 (Suppl. 577), 5–9 (1997).
11. Ellis, H. et al. Adhesion-related hospital readmissions after abdominal and pelvic surgery: a retrospective cohort study. Lancet 353, 1476–1480 (1999).
12. Menzies, D. & Ellis, H. Intestinal obstruction from adhesions–how big is the problem? Ann. R. Coll. Surg. Engl. 72, 60–63 (1990).
13. Parker, M.C. et al. Colorectal surgery: the risk and burden of adhesion-related complications. Colorectal Dis. 6, 506–511 (2004).
14. Ghellai, A.M. et al. Role of transforming growth factor-b1 in peritonitis-induced adhesions. J. Gastrointest. Surg. 4, 316–323 (2000).
15. Chung, D.R. et al. $CD4^+$ T cells regulate surgical and postinfectious adhesion formation. J. Exp. Med. 195, 1471–1478 (2002).
16. Bendelac, A., Savage, P.B. & Teyton, L. The biology of NKT cells. Annu. Rev. Immunol. 25, 297–336 (2007).
17. Taniguchi, M., Harada, M., Kojo, S., Nakayama, T. & Wakao, H. The regulatory role of Va14 NKT cells in innate and acquired immune response. Annu. Rev. Immunol. 21, 483–513 (2003).
18. Yoshimoto, T. & Paul, W.E. $CD4^{pos}$, $NK1.1^{pos}$ T cells promptly produce interleukin 4 in response to in vivo challenge with anti-CD3. J. Exp. Med. 179, 1285–1295 (1994).
19. Cui, J. et al. Requirement for Va14 NKT cells in IL-12–mediated rejection of tumors. Science 278, 1623–1626 (1997).
20. Meraz, M.A. et al. Targeted disruption of the Stat1 gene in mice reveals unexpected physiologic specificity in the JAK-STAT signaling pathway. Cell 84, 431–442 (1996).
21. Kawano, T. et al. Natural killer–like nonspecific tumor cell lysis mediated by specific ligand-activated Va14 NKT cells. Proc. Natl. Acad. Sci. USA 95, 5690–5693 (1998).
22. Kaplan, M.H., Sun, Y.L., Hoey, T. & Grusby, M.J. Impaired IL-12 responses and enhanced development of T_H2 cells in Stat4-deficient mice. Nature 382, 174–177 (1996).
23. Takeda, K. et al. Essential role of Stat6 in IL-4 signalling. Nature 380, 627–630 (1996).
24. Katayama, I. & Nishioka, K. Substance P augments fibrogenic cytokine-induced fibroblast proliferation: possible involvement of neuropeptide in tissue fibrosis. J. Dermatol. Sci. 15, 201–206 (1997).
25. Zimmer, A. et al. Hypoalgesia in mice with a targeted deletion of the tachykinin 1 gene. Proc. Natl. Acad. Sci. USA 95, 2630–2635 (1998).
26. Holmdahl, L., Eriksson, E., al-Jabreen, M. & Risberg, B. Fibrinolysis in human peritoneum during operation. Surgery 119, 701–705 (1996).
27. Kuroiwa, T. et al. Hepatocyte growth factor ameliorates acute graft-versus-host disease and promotes hematopoietic function. J. Clin. Invest. 107, 1365–1373 (2001).
28. Ido, A., Numata, M., Kodama, M. & Tsubouchi, H. Mucosal repair and growth factors: recombinant human hepatocyte growth factor as an innovative therapy for inflammatory bowel disease. J. Gastroenterol. 40, 925–931 (2005).
29. Kennedy, R., Costain, D.J., McAlister, V.C. & Lee, T.D. Prevention of experimental postoperative peritoneal adhesions by N,O-carboxymethyl chitosan. Surgery 120, 866–870 (1996).
30. Kocak, I., Unlu, C., Akcan, Y. & Yakin, K. Reduction of adhesion formation with cross-linked hyaluronic acid after peritoneal surgery in rats. Fertil. Steril. 72, 873–878 (1999).

Available online at www.sciencedirect.com
ScienceDirect
Parasitology International 57 (2008) 54–61
www.elsevier.com/locate/parint

Change of subunit composition of mitochondrial complex II (succinate–ubiquinone reductase/quinol–fumarate reductase) in *Ascaris suum* during the migration in the experimental host

Fumiko Iwata [a,b], Noriko Shinjyo [a], Hisako Amino [a], Kimitoshi Sakamoto [a], M. Khyrul Islam [c], Naotoshi Tsuji [c], Kiyoshi Kita [a,*]

[a] *Department of Biomedical Chemistry, Graduate School of Medicine, The University of Tokyo, 7-3-1 Hongo, Bunkyo-ku, Tokyo 113 0033, Japan*
[b] *Department of Molecular and Cellular Physiology, Graduate School of Comprehensive Human Sciences, University of Tsukuba, Tsukuba, Japan*
[c] *Laboratory of Parasitic Diseases, National Institute of Animal Health, National Agriculture Research Organization, Tsukuba, Japan*

Received 13 July 2007; received in revised form 11 August 2007; accepted 16 August 2007
Available online 25 August 2007

Abstract

The mitochondrial metabolic pathway of the parasitic nematode *Ascaris suum* changes dramatically during its life cycle, to adapt to changes in the environmental oxygen concentration. We previously showed that *A. suum* mitochondria express stage-specific isoforms of complex II (succinate–ubiquinone reductase: SQR/quinol–fumarate reductase: QFR). The flavoprotein (Fp) and small subunit of cytochrome *b* (CybS) in adult complex II differ from those of infective third stage larval (L3) complex II. However, there is no difference in the iron–sulfur cluster (Ip) or the large subunit of cytochrome *b* (CybL) between adult and L3 isoforms of complex II. In the present study, to clarify the changes that occur in the respiratory chain of *A. suum* larvae during their migration in the host, we examined enzymatic activity, quinone content and complex II subunit composition in mitochondria of lung stage L3 (LL3) *A. suum* larvae. LL3 mitochondria showed higher QFR activity (~160 nmol/min/mg) than mitochondria of *A. suum* at other stages (L3: ~80 nmol/min/mg; adult: ~70 nmol/min/mg). Ubiquinone content in LL3 mitochondria was more abundant than rhodoquinone (~1.8 nmol/mg versus ~0.9 nmol/mg). Interestingly, the results of two-dimensional bule-native/sodium dodecyl sulfate polyacrylamide gel electrophoresis analyses showed that LL3 mitochondria contained larval Fp (Fp^L) and adult Fp (Fp^A) at a ratio of 1:0.56, and that most LL3 CybS subunits were of the adult form ($CybS^A$). This clearly indicates that the rearrangement of complex II begins with a change in the isoform of the anchor CybS subunit, followed by a similar change in the Fp subunit.

Keywords: *Ascaris suum* lung-stage L3 (LL3); Complex II; Quinone; NADH–fumarate reductase; Quinol–fumarate reductase (QFR); Oxidative stress

1. Introduction

During the life cycle of the parasitic nematode *Ascaris suum*, it transitions from aerobic to anaerobic metabolism in parallel with changes in the environmental oxygen concentration (Fig. 1) [1–6]. In aerobic metabolism, which is used by *A. suum* larvae during their development from fertilized egg to third stage larvae (L3), phosphoenolpyruvate (PEP) is converted to pyruvate by pyruvate kinase, and pyruvate is converted to CO_2 and H_2O via the tricarboxylic acid (TCA) cycle, generating a large amount of ATP by aerobic oxidative phosphorylation [7]. Adult *A. suum* worms, which live in a low-oxygen environment, use the anaerobic phosphoenolpyruvate carboxykinase (PEPCK)-

Abbreviations: Fp, flavoprotein subunit; Ip, iron–sulfur cluster subunit; CybL, large subunit of cytochrome *b*; CybS, small subunit of cytochrome *b*; Fp^L, larval Fp; Fp^A, adult Fp; $CybS^L$, larval CybS; $CybS^A$, adult CybS; L3, third stage larva; LL3, lung stage L3; SDH, succinate dehydrogenase; SQR, succinate–ubiquinone reductase; QFR, quinol–fumarate reductase; UQ, ubiquinone; dUQ, decyl UQ; RQ, rhodoquinone; dRQ, decyl RQ; HPLC, high performance liquid chromatography; BN-PAGE, blue-native polyacrylamide gel electrophoresis; SDS-PAGE, sodium dodecyl sulfate-PAGE; CBB, Coomassie brilliant blue.

* Corresponding author. Tel.: +81 3 5841 3526; fax: +81 3 5841 3444.
E-mail address: kitak@m.u-tokyo.ac.jp (K. Kita).

1383-5769/$ - see front matter © 2007 Elsevier Ireland Ltd. All rights reserved.
doi:10.1016/j.parint.2007.08.002

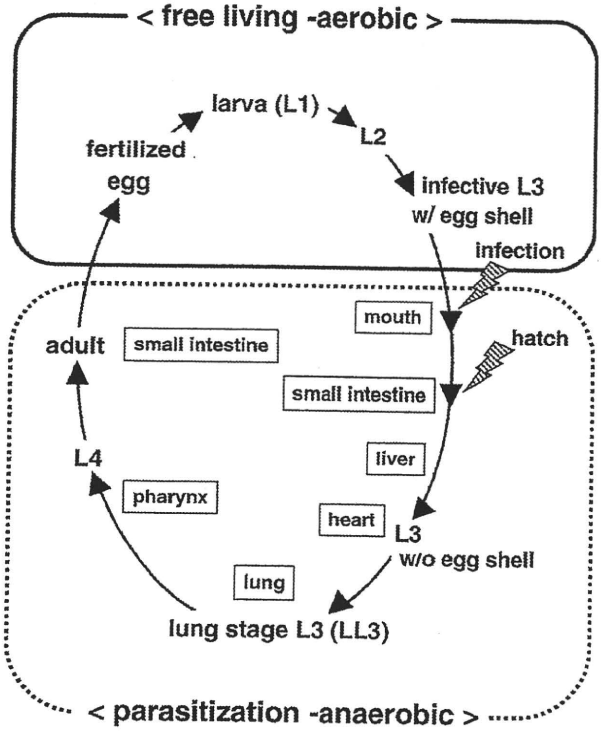

Fig. 1. Life cycle of *Ascaris suum*. Fertilized eggs grow to infective L3 under aerobic environment. Infective L3 larvae are ingested by the host, reach the small intestine and hatch there. Afterwards, larvae migrate into the host body (liver, heart, lung, pharynx), and finally migrate back to the small intestine and become adults. In the host small intestine, the oxygen concentration is only 2.5 to 5% of that of the exogenous environment [12]. w/, with; w/o, without.

succinate pathway. In the first step in the PEPCK-succinate pathway, PEPCK fixes CO_2 to PEP in the cytosol, to form oxaloacetate. This oxaloacetate is then reduced to malate, which is dismutated in mitochondria. Then, fumarate hydratase converts the malate to fumarate, which is reduced by the quinol–fumarate reductase (QFR) activity of complex II; in aerobic respiration, complex II catalyzes oxidation of succinate (succinate–ubiquinone reductase; SQR) in the mitochondria. The last step of the PEPCK-succinate pathway involves the NADH–fumarate reductase system, which is composed of complex I (NADH–quinone reductase), low-potential rhodoquinone (RQ) and complex II (QFR) [3,8]. Electron transfer from NADH to fumarate is coupled to ATP synthesis by site I phosphorylation in complex I. The difference in redox potential between NAD^+/NADH ($Em' = -320$ mV) and fumarate/succinate ($Em' = +30$ mV) is sufficient to drive ATP synthesis.

In eukaryotes, complex II is localized in the inner mitochondrial membrane, and is generally composed of 4 peptides [3]. The largest flavoprotein (Fp) subunit has an approximate molecular mass of 70 kDa and contains flavin adenine dinucleotide (FAD) as a prosthetic group. The relatively hydrophilic catalytic region of complex II is formed by the Fp subunit and the iron–sulfur cluster (Ip) subunit, whose molecular weight is about 30 kDa. The remaining subunits comprise cytochrome *b*, which contains heme *b*. Cytochrome *b* is composed of 2 hydrophobic membrane-anchoring polypeptide subunits; the 15-kDa large subunit (CybL) and the 13-kDa small subunit (CybS). These cytochrome *b* subunits are necessary for interaction between complex II and hydrophobic membrane-associated quinones such as ubiquinone (UQ) and RQ. However, it is unclear how heme *b* is involved in the electron transfer between complex II and quinones.

In a previous study, we showed that *A. suum* mitochondria express stage-specific isoforms of complex II [5,6,9]. While there is no difference in the isoforms of the Ip and CybL subunits of complex II between L3 larvae and adult *A. suum*, they have different isoforms of the complex II subunits Fp (larval, Fp^L; adult, Fp^A) and CybS (larval, $CybS^L$; adult, $CybS^A$). Quinone species in the mitochondria also change during the life cycle of *A. suum*. In adult mitochondria, the predominant quinone is the low-potential rhodoquinone (RQ; $Em' = -63$ mV); in larvae, the predominant quinone is ubiquinone (UQ; $Em' = +110$ mV) [10]. A combination of SQR and UQ, and that of QFR and a low-potential quinone, such as RQ or menaquinone (MK), is also observed in *E. coli* and other bacteria during metabolic adaptation to changes in oxygen supply [11]. UQ has a higher potential than RQ; therefore, RQ is better suited to transferring electrons to fumarate than is UQ. In L2 and L3 *A. suum* larvae, UQ preferentially donates electrons to the cytochrome chain in the mitochondria. Thus, UQ participates in aerobic metabolism in *A. suum* larvae, whereas RQ participates in anaerobic metabolism in adult *A. suum*.

After ingestion by the definitive host, the L3 larvae penetrate the intestinal wall and reach to the lung migrating through the tissues such as liver and heart. The L3 larvae passes from lung via the trachea to the small intestine where they molt to L4 and develop into sexually maturate adult worms in the small intestine [12]. Although studies have shown a clear difference in energy metabolism between larval and adult *A. suum* mitochondria, little is known about changes in the properties of mitochondria (including respiration) during migration of *A. suum* larvae in the host.

In the present study, we examined changes in subunit composition of *A. suum* larval complex II from lung stage L3 (LL3) larvae obtained from rabbits. Enzymatic analyses showed that properties of LL3 mitochondria differed from those of L3 and adult mitochondria. Protein chemical analysis revealed that the change in complex II begins with the anchor CybS subunit, and then occurs in the Fp subunit.

2. Materials and methods

2.1. Parasites

A. suum adult worms were procured from a slaughterhouse in Tokyo, Japan. Third stage infective (L3) larvae and lung stage L3 (LL3) larvae were obtained as previously described [5,13]. All animals used in this study were acclimatized to the experimental conditions for 2 weeks before the experiment. Animal experiments were conducted in accordance with the protocols approved by the Animal Care and Use Committee, National

Institute of Animal Health (Approval nos. 589,712). For the preparation of LL3 larvae, Japanese white rabbits were made to ingest infective *A. suum* eggs (approximately 1.5×10^5 eggs per rabbit), and infected lungs were removed from the rabbits 7 days after ingestion of the eggs. The lungs were cut into 2-cm cubes using a razor blade, and the cubes were put into nylon mesh bags (KA1000, Eiken Kizai, Tokyo, Japan) in 50-ml polypropylene conical tubes filled with phosphate-buffered saline (PBS) containing 100 μg/ml penicillin and 100 μg/ml streptomycin. Those tubes were then kept in a humidified incubator at 37 °C for 4 to 5 h. During that incubation, the larvae dropped out of the bags into the bottom of the tubes. The larvae were then washed several times with fresh PBS in a 37 °C water bath. Contaminating erythrocytes from the host rabbits were eliminated by hemolysis, which was induced by washing the pellet containing LL3 larvae with pre-warmed tap water at 37 °C. The body length of the LL3 larvae, obtained from infected rabbit on day 7 post-infection, were 1.2–1.3 mm. They were slightly smaller than LL3 larvae derived from infected swine at the same post-infectious stage (1.5 mm) [14].

2.2. Preparation of mitochondria from L3, LL3 and adult A. suum

Mitochondria from L3 and adult *A. suum* muscle were prepared using the method described by Amino et al. [5]. Because that method was not applicable to LL3 mitochondria, we established the following method to obtain active mitochondria from LL3; the entire procedure was performed on ice or at 4 °C. The LL3 larvae were gently suspended in an equal volume of ice-cold suspension buffer containing 210 mM mannitol, 10 mM sucrose, 1 mM disodium EDTA and 50 mM Tris–HCl (pH 7.5), supplemented with 10 mM sodium malonate [15]. The LL3 larvae in the suspension were cut using a scalpel (No. 10 blade, Feather, Osaka, Japan) on a 90 × 75 × 3-mm custom-made glass plate with a hollow (diameter, 22 mm; depth, 3 mm) in the middle. The cut larvae were then homogenized with a hand-powered glass–glass homogenizer for 15 min, and the homogenate was centrifuged at 500 × g for 1 min. The resulting supernatant was centrifuged at 10,000 × g for 10 min to obtain the mitochondrial pellet. The pellet was resuspended in the suspension buffer and stored at −80 °C until used. The protein concentration of the mitochondria was determined using the method of Lowry [16], using bovine serum albumin as the standard.

2.3. Enzyme assay

All assays were performed at 25 °C, using 50 mM potassium phosphate (pH 7.5) as the reaction buffer. The SQR [17], succinate dehydrogenase (SDH) [18], QFR [19] and NADH–fumarate reductase [8] activities of mitochondria were assayed as described. The NADH-decyl UQ (-dUQ) and NADH-decyl RQ (-dRQ) assays were performed using the same method as the NADH–fumarate reductase activity assay, except that 60 μM dUQ or dRQ was used as the electron acceptor, instead of sodium fumarate.

2.4. Quantitative analysis of quinone in LL3 mitochondria

Quinones were extracted from lyophilized LL3 mitochondria, and were analyzed by reverse-phase HPLC as described by Miyadera et al. [20]. The concentrations of quinones were determined spectrophotometrically using the following extinction coefficients: for UQ, $E_{1\%1\ cm}$ at 275 nm = 158; for RQ, $E_{1\%1\ cm}$ at 283 nm = 141 [10].

2.5. Western blotting

Complex II from L3, LL3 and adult mitochondria was analyzed by Western blotting using the method of Towbin et al. [21]. The mitochondrial proteins were separated by SDS-PAGE, using a 7.5% acrylamide gel for the Fp subunit, and using a 10/20% gradient acrylamide gel (Daiichi, Tokyo, Japan) for the Ip and CybS subunits. The proteins were then transferred to a nitrocellulose membrane at 4 °C and 80 V for 1 h. The membranes were incubated with the following antibodies in Tris-buffered saline containing 0.05% (w/v) Tween 20 (TBST) and 2% (w/v) skim milk: anti-Fp monoclonal, diluted 1:3000 [18]; anti-$CybS^A$ monoclonal, diluted 1:5000 [5]; $CybS^L$ peptide-based polyclonal, diluted 1:300 [5]; mixture of anti-Ip and anti-CybS polyclonal, diluted 1:2000 [5]. Each membrane was then incubated for 30 min with one of the following alkaline phosphatase-conjugated secondary antibodies: goat anti-mouse IgG (for Fp and $CybS^A$), or goat anti-rabbit IgG (for $CybS^L$, Ip and CybS). The proteins were detected using the alkaline phosphatase method. The amount of protein was normalized to the intensity of the Ip subunit at each stage, using NIH Image (a free image analyzing program for the Macintosh, developed by National Institutes of Health (NIH); www.rsb.info.nih.gov/nih-image/download.html).

2.6. Solubilization of mitochondria for blue native (BN-) PAGE

Mitochondria from L3, LL3 and adult *A. suum* (1.5 μmol/min in SDH activity) were incubated on ice for 1 h in 0.5% (w/v) sucrose monolaurate (SML) and Native PAGE™ sample buffer containing 50 mM Bis–Tris, 6 N HCl, 50 mM NaCl, 10% (w/v) glycerol and 0.001% (w/v) Ponceau S in 10 mM Tris–HCl (pH 7.5) (User manual, version A 2006; www.invitrogen.com/content/sfs/manuals/nativepage_man.pdf, Invitrogen, Carlsbad, CA, USA). They were then ultracentrifuged at 200,000 × g and 4 °C for 1 h, and the resulting supernatant was subjected to BN-PAGE, as described below.

2.7. BN-PAGE, CBB staining, in-gel SDH activity staining and Western blotting

The solubilized mitochondria were subjected to BN-PAGE [22] using Native PAGE Novex 4–16% Bis–Tris gels (Invitrogen). Electrophoresis was performed at 4 °C, at 150 V for 1 h, and then at 250 V, voltage constant. The cathode and anode buffers were prepared according to the user's manual of the Native PAGE Novex Bis–Tris gel system. Following the BN-PAGE, CBB staining was performed according to the user's

manual. The SDH activity of mitochondrial protein of L3, LL3 and adult *A. suum* was detected as described elsewhere [18,23]. After the BN-PAGE (first dimension), the gel cut by lane from the first-dimensional gel was equilibrated with SDS-PAGE buffer, and was then loaded onto the second-dimensional gel (7.5% acrylamide gel for Fp, and 10/20% gradient acrylamide gels (Daiichi) for Ip and CybS). The subsequent analysis by Western blotting was performed as described above.

3. Results

3.1. Enzymatic properties of LL3 complex II

Because only a small amount of LL3 larvae was obtained, and because LL3 larvae were more resistant to homogenization than L3 larvae and adult worms, we tried to establish a specific and reproducible protocol for the preparation of mitochondria from LL3 larvae. We found that cutting LL3 larvae with a scalpel was an effective method of recovering active mitochondria. Using the established protocol, we obtained approximately 0.5 mg of mitochondria from 1 infected rabbit. Fig. 2 shows the results of comparative analysis of enzyme activities, relative to NADH–fumarate reductase activity, in L3, LL3 and adult mitochondria.

The Fp and Ip subunits form the hydrophilic catalytic portion of complex II, and act as a succinate dehydrogenase (SDH), catalyzing the oxidation of succinate by the water-soluble electron acceptor phenazine methosulfate. The L3 and LL3 mitochondria had almost identical levels of SDH activity, whereas the SDH activity of adult mitochondria was 2.7 to 3.9 times higher than that of L3 and LL3 mitochondria (Fig. 2A). SQR catalyzes electron transfer from succinate to the physiological electron acceptor, ubiquinone. Similarly, SQR activity of adult mitochondria was 1.8 to 3.9 times higher than that of L3 and LL3 mitochondria (Fig. 2B). QFR catalyzes a reaction that is the reverse of the reaction catalyzed by SQR. The QFR activity of LL3 mitochondria was higher than that of L3 and adult mitochondria (Fig. 2C). The NADH–fumarate

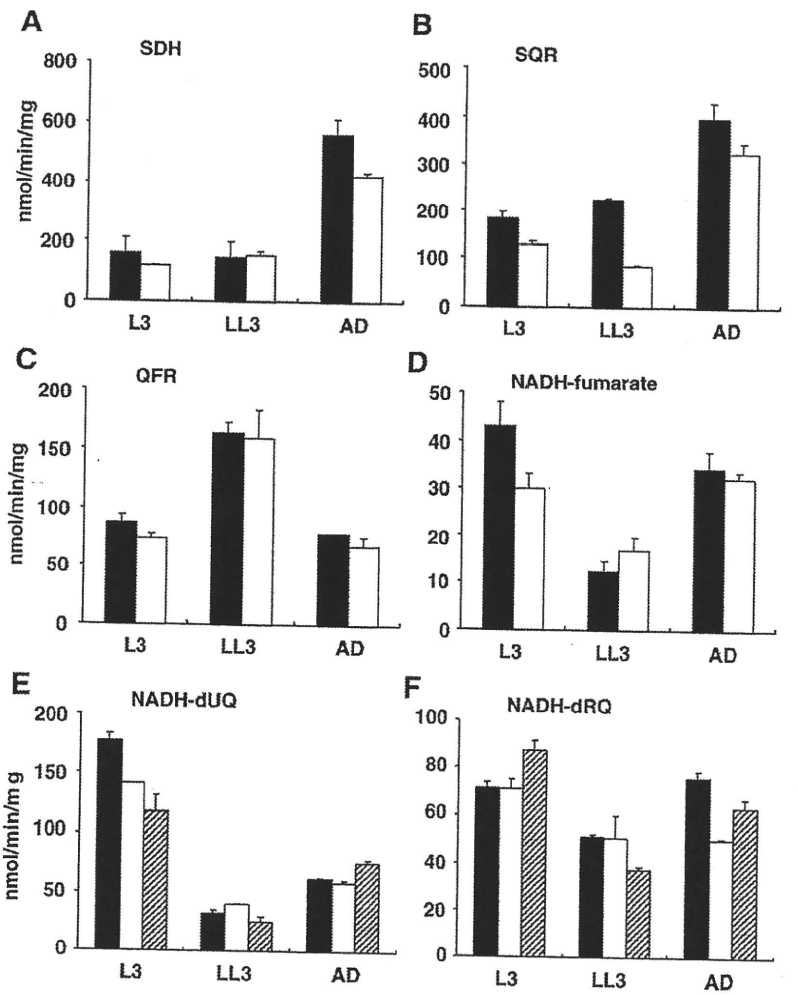

Fig. 2. Enzyme assay. Enzyme activities of complex I and II of mitochondria from L3 *A. suum* larvae, LL3 *A. suum* larvae, and *A. suum* adults. (A) SDH, (B) SQR, (C) QFR, (D) NADH–fumarate reductase, (E) NADH-dUQ and (F) NADH-dRQ. The mean and standard error were derived from triplicate measurements. Solid bars indicate experiment 1; open bars indicates experiment 2; stripe bars indicate experiment 3. Assays were performed as in materials and methods.

reductase system is an anaerobic electron-transport system of mitochondria, and is the terminal step of the PEPCK-succinate pathway. In the NADH–fumarate reductase system, the reducing equivalent of NADH is transferred to the low-potential RQ by the NADH-RQ reductase complex (Complex I). This pathway ends with the production of succinate by the rhodoquinol-fumarate reductase activity of complex II. Unexpectedly, the NADH–fumarate reductase activity of LL3 mitochondria was lower than that of L3 and adult mitochondria (Fig. 2D). The NADH-dUQ and NADH-dRQ activities of LL3 mitochondria were lower than those of L3 and adult mitochondria (Fig. 2E and F), suggesting that the low NADH–fumarate reductase activity of LL3 mitochondria is due to the lower activity of complex I in LL3 mitochondria.

3.2. Quinone components in LL3 mitochondria

Because quinone species are important low-molecular-weight mediators of electron transfer between respiratory enzymes, and because the ratio between RQ and UQ seems to be a critical factor in the direction of electron transfer in the chain, we examined the quinone content of LL3 mitochondria complex II. Although the amount of LL3 mitochondria that we obtained was quite limited, we performed the analysis using 2 different samples of LL3 mitochondria. The first sample of LL3 mitochondria contained 1.68 nmol/mg UQ-9 and 0.85 nmol/mg RQ-9. A similar result was obtained for the second sample (Table 1), indicating that the UQ content of LL3 mitochondria is approximately 2-fold greater than that of RQ. It should be noted that UQ-9 is the predominant quinone of L3 complex II (75% of the total quinone content), and that RQ is the only quinone present in complex II from adult *A. suum* muscle [10].

3.3. Subunit composition of the LL3 mitochondria complex II

To examine the subunit structure of complex II in LL3 mitochondria, we performed Western blotting. Because the isoforms of the Ip and CybL subunits do not change during the *A. suum* life cycle [5], the amount of proteins used for the Western blotting of Fp and CybS subunits was normalized to the intensity of the Ip subunit, which was visualized using the alkaline phosphatase method (Fig. 3D). LL3 mitochondrial complex II contained both Fp^L and Fp^A (Fig. 3). The LL3 and adult complex II had a Fp^L:Fp^A band intensity ratio of 1:0.56 and 1:3.5, respectively, whereas only the Fp^L band was observed in blots of L3 complex II (Fig. 3A). For the $CybS^A$ subunit, the

Table 1
Quinone quantitative analysis of LL3 mitochondria

	(nmol/mg)		Ratio
Experiment	UQ-9[a]	RQ-9[b]	UQ-9[a]:RQ-9[b]
1	1.68	0.85	1.98:1
2	1.89	1.00	1.89:1

[a] UQ-9, ubiquinone-9.
[b] RQ-9, rhodoquinone-9.

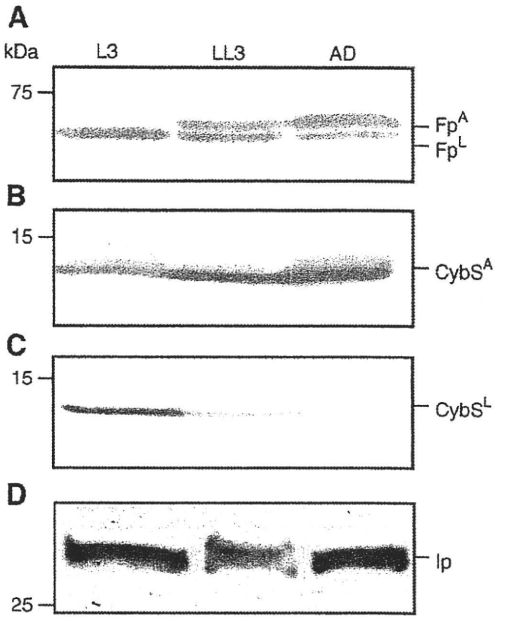

Fig. 3. Western blotting. Western blotting with (A) *A. suum* Fp monoclonal antibody, diluted 1:3000. (B) Monoclonal antibody against $CybS^A$ diluted 1:5000, and (C) Peptide-based polyclonal antibody against $CybS^L$ diluted 1:300. Protein levels were normalized to the Ip band intensity using (D) mixture of anti-Ip and anti-CybS polyclonal antibody diluted 1:2000. L3, *A. suum* larvae prepared from embryonated eggs; LL3, lung-stage L3; AD, *A. suum* adult. Precision Plus All Blue Standard (BIO-RAD).

L3:LL3:adult band intensity ratio was 1:3.5:6.1 (Fig. 3B). Only a small amount of $CybS^L$ was detected in LL3 mitochondria (<5% of $CybS^L$ in L3 mitochondria), and no $CybS^L$ was found in adult mitochondria (Fig. 3C). This result was reproducible in more than 3 experiments, suggesting that the subunit isoform change of LL3 complex II starts with CybS, and then occurs in Fp.

Because Western blotting clearly showed a difference in timing of isoform change between Fp and CybS subunits during migration in the host, we used BN-PAGE to examine the subunit composition of functional complex II. Mitochondrial proteins of each stage solubilized with sucrose monolaurate were subjected to BN-PAGE, and were then stained for CBB (Fig. 4A) or SDH activity (Fig. 4B) in the gel. Complex II from all 3 stages exhibited SDH activity in the gel, and band intensities of the 3 stages were almost identical when the amount of protein was normalized to 1.5 μmol/min SDH activity.

Next, we performed two-dimensional electrophoresis; with BN-PAGE as the first dimension, and SDS-PAGE as the second dimension. After the BN-PAGE, the gel was cut and was horizontally loaded onto SDS-PAGE. Following the two-dimensional electrophoresis, proteins were analyzed by Western blotting (Fig. 4C). Spots of Fps and CybSs were found in the same position as the SDH-stain band, indicating that native complex II with 4 subunits migrated during electrophoresis in the presence of the detergent. No extra spot was found in an area different from the SDH-stain position. In addition, the patterns

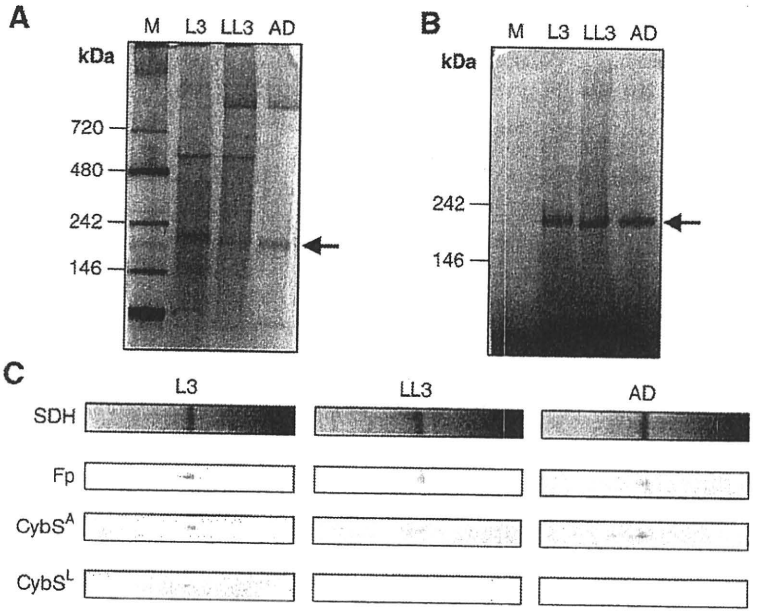

Fig. 4. BN-PAGE analysis. BN-PAGE analysis of mitochondria from *A. suum* L3 larvae, LL3 larvae and adults (1.5 μmol/min SDH activity). (A) CBB-stain. Arrow indicates expected SDH active bands. (B) SDH activity stained in gels of Native PAGE™ Bis–Tris gel (4–16%). Arrow shows SDH active bands. (C) Western blotting after SDS-PAGE, following BN-PAGE. Antibodies used were the same as in Fig. 3. The size marker is Native Mark Unstained Protein Standard (Invitrogen).

of intensity of the spots in Fig. 4C were almost identical to the results of Western blotting after SDS-PAGE (Fig. 3).

4. Discussion

In the present study, biochemical analyses of mitochondrial complex II were performed to elucidate how complex II in *A. suum* mitochondria change its isoform composition during migration in the mammalian host. In the first step of this study, we examined complex II from LL3 larvae (Fig. 1), because there is an established method of sample collection from rabbit lung, and because several properties of LL3 have been well studied [13,24]. The natural host of *A. suum* is swine so that we need pigs for developing the migratory phase and the adult stages. However, pig rearing facilities are currently quite limited for the purpose of doing *Ascaris* infection. Helminth researchers have previously examined the life cycle and worm burdens in rabbits [25,26]. The results showed that several criteria such as the organ migratory routes and recovery of larvae in rabbits were quite similar to those in pigs, indicating that rabbit can be fairly used for permissive hosts. Actually, *Ascaris* researchers including our group have employed rabbits to do biochemical experiments of the roundworms [27,28].

We previously demonstrated that *A. suum* mitochondria express stage-specific isoforms of complex II; i.e., the flavoprotein subunit (Fp) and the small subunit of cytochrome *b* (CybS) of complex II isolated from L3 infective eggs differ from those of adult muscle complex II, while the 2 forms of complex II have an identical iron-sulfur cluster subunit (Ip) and large subunit of cytochrome *b* (CybL). Therefore, the subunit isoform composition of complex II must change during migration in the host. To our surprise, Western blot analyses showed that both the Fp^L and Fp^A isoforms (in the ratio of 1: 0.56) were present in LL3 mitochondria, while the majority of CybS subunit was of the isoform $CybS^A$ (Fig. 3A and B). This means that expression of adult Fp does not synchronize with that expression of adult CybS, and suggests that LL3 complex II has a different combination of subunit isoforms than L3 and adult complex II.

To analyze the native state of complex II subunit composition in LL3 mitochondria, we used BN-/SDS-PAGE two-dimensional electrophoresis (Fig. 4C). The spots of the subunits were found at the same position as the SDH bands,

Table 2
Enzyme activities of L3, LL3 and adult complex I and II of *Ascaris suum* mitochondria

Assay	Experiment	Specific activity (nmol/min/mg)		
		L3	LL3	Adult
SDH	1	158±36	145±16	566±15
(complex II)	2	118±5.6	152±25	424±22
SQR	1	184±28	224±8.3	400±63
(complex II)	2	129±16	84.1±4.0	326±43
QFR	1	87.8±6.0	164±8.6	78.5±0.058
(complex II)	2	73.5±7.6	159±47	66.8±16
NADH–fumarate	1	43.0±10	12.3±4.4	34.4±7.1
reductase (complex I,II)	2	30.1±6.4	16.7±5.6	32.3±2.6
NADH-dUQ	1	177±12	32.3±5.6	62.4±1.9
	2	141±0.92	39.8±1.9	58.6±4.6
(complex I)	3	118±26	24.8±8.8	76.3±4.9
NADH-dRQ	1	71.4±4.4	51.6±2.0	75.7±5.6
	2	71.0±7.8	51.0±18	50.3±1.3
(complex I)	3	87.1±8.5	37.6±2.4	63.4±7.6

without any extra spots. This result indicates that the spots detected were derived from active complex II consisting of 4 subunits. In LL3 mitochondria, all 4 larva-/adult-types of Fp-CybS subunits was observed, while Fp^L, $CybS^A$ and $CybS^L$ subunit isoforms were detected in L3 mitochondria, and Fp^L, Fp^A and $CybS^A$ subunit isoforms were detected in adult mitochondria. The pattern of the intensity of the spots in Fig. 4C is consistent with that of the Western blotting after SDS-PAGE (Fig. 3), indicating that mitochondrial complex II subunit switching first occurs in CybS, and then occurs in Fp, during migration in the host.

Of the 4 possible Fp-CybS subunit combinations (Fp^L-$CybS^A$, Fp^A-$CybS^A$, Fp^L-$CybS^L$ and Fp^A-$CybS^L$), Fp^L-$CybS^A$ is the predominant combination in LL3 mitochondria. Western blot analysis of young adult mitochondria obtained from the muscle of 12-cm-long female worms showed that $CybS^L$ had completely disappeared, whereas Fp^L remained at a ratio of Fp^L:Fp^A = 1:1.5 (data not shown), although only 1 SDH band was observed in BN-PAGE. This finding may be due to similar properties between the 2 complexes with different combinations.

However, several questions remain unanswered. Because of limited sample amount, it is difficult to purify complex II from LL3 mitochondria. Reports indicate that adult *A. suum* uses the NADH–fumarate reductase system in its anaerobic host environment; in the NADH–fumarate reductase system, the QFR activity of mitochondrial complex II plays a significant role [3,29,30]. However, we previously found that L3 complex II had higher QFR activity than adult complex II, and presumed that this was due to pre-adaptation to the dramatic change in oxygen availability during infection of the host [5]. In the present study, we found that the QFR activity of LL3 complex II was twice as high as that of L3 complex II (Fig. 2C, Table 2). The host lung is a relatively aerobic environment (13.2% O_2) [31], suggesting that the larvae pre-adapt before they migrate into the anaerobic environment of the host small intestine (5% O_2).

Although LL3 mitochondria showed the highest QFR activity of the 3 stages we examined, their NADH–fumarate reductase activity was unexpectedly low (Fig. 2D). This appears to be due to the effects of low complex I activity, as indicated by the NADH-dUQ and NADH-dRQ assays (Fig. 2E and F). The NADH–fumarate reductase system is composed of complex I (initial dehydrogenase of NADH), RQ (electron mediator), and complex II (terminal oxidase for fumarate reduction). We also examined the quinone content of the mitochondria. Analysis of the quinone contents of mitochondria isolated from unembryonated eggs, L3 larvae and adult muscle showed that the predominant quinone in larval mitochondria (which possess an aerobic respiratory chain) was UQ-9 (75% of the total quinone content) [10]. In contrast, the only quinone present in anaerobic mitochondria from adult muscle is RQ-9. Consistent with these findings, reconstitution studies using bovine heart complex I and adult *A. suum* QFR show that RQ is essential for the function of the NADH–fumarate reductase system [32]. Specifically, when RQ-9 was incorporated into the system, the maximum activity of reconstituted NADH–fumarate reductase activity was 430 nmol/min/mg of *A. suum* complex II, while no activity was observed in the presence of UQ-9. In addition, our previous findings suggest that although *A. suum* adult complex I uses both RQ and UQ as electron acceptors, the 2 quinones have different ways of binding reaction and reaction with *A. suum* complex I [33]. It should be noted that in the present study, UQ accounted for 66% of the total quinone of LL3 complex II, which is an intermediate between those of L3 and adult complex II [10]. Further analysis of the effect of endogenous quinones in the mitochondria of the enzyme activities of complex I and complex II is needed to elucidate the unique properties of the NADH–fumarate reductase system of *A. suum*.

In the present study, we examined how mitochondrial complex II of *A. suum* changes its subunit composition, especially during migration in the host. We found that the small subunit of cytochrome *b* (CybS) starts to change its isoform before the flavoprotein (Fp) subunit does so. Further clarification of this process will require analysis of larvae from other migration stages in the host. In each stage, the metabolic pathway of *A. suum* may continue to change according to the environmental changes, even in the host body. To elucidate this dynamic change in the mitochondrial respiratory system of *A. suum* during migration, we plan to establish an experimental system using swine, which is a definitive host of *A. suum*. With such a system, further biochemical analysis should reveal novel properties of complex II in LL3 mitochondria.

Acknowledgements

We thank Dr. Tetsuro Ishii for his academic support. This study was supported by a grant-in-aid for scientific research on Priority Areas, for the 21st Century COE Program (F-3) and for Creative Scientific Research from the Japanese Ministry of Education, Science, Culture, Sports and Technology (180 73004, 18GS0314).

References

[1] Komuniecki R, Komuniecki PR. Aerobic–anaerobic transitions in energy metabolism during the development of the parasitic nematode *Ascaris suum*. In: Boothroyd JC, Komuniecki R, editors. Molecular approaches to parasitology. New York: Wiley-Liss; 1995.

[2] Tielens AGM, Rotte C, van Hellemond JJ, Martin W. Mitochondria as we don't know them. Trends Biochem Sci 2002;27:56–72.

[3] Kita K, Takamiya S. Electron-transfer complexes in *Ascaris* mitochondria. Adv Parasitol 2002;51:95–131.

[4] Kita K. Electron-transfer complexes in *Ascaris suum*. Parasitol Today 1992;8: 155–9.

[5] Amino H, Osanai A, Miyadera H, Shinjyo N, Tomitsuka E, Taka H, et al. Isolation and characterization of the stage-specific cytochrome *b* small subunit (CybS) of *Ascaris suum* complex II from the aerobic respiratory chain of larval mitochondria. Mol Biochem Parasitol 2003;128: 175–86.

[6] Amino H, Wang H, Hirawake H, Saruta F, Mizuchi D, Mineki R, et al. Stage-specific isoforms of *Ascaris suum* complex II: the fumarate reductase of the parasitic adult and the succinate dehydrogenase of free-living larvae share a common iron–sulfur subunit. Mol Biochem Parasitol 2000;106: 63–76.

[7] Kita K, Hirawake H, Miyadera H, Amino H, Takeo S. Role of complex II in anaerobic respiration of the parasite mitochondria from *Ascaris suum* and *Plasmodium falciparm*. Biochim Biophys Acta 2002;1553: 123–39.

[8] Omura S, Miyadera H, Ui H, Shiomi K, Yamaguchi Y, Masuma R, et al. An anthelmintic compound, nafredin, shows selective inhibition of

complex I in helminth mitochondria. Proc Natl Acad Sci U S A 2001;98: 60–2.
[9] Saruta F, Kuramochi T, Nakamura K, Takamiya S, Yu Y, Aoki T, et al. Stage-specific isoforms of complex II (succinate–ubiquinone oxidoreductase) in mitochondria from the parasitic nematode, *Ascaris suum*. J Biol Chem 1995;270:928–32.
[10] Takamiya S, Kita K, Wang H, Weinstein PP, Hiraishi A, Oya H, et al. Developmental changes in the respiratory chain of *Ascaris* mitochondria. Biochim Biophys Acta 1993;1141:65–74.
[11] Cole ST, Condon C, Lemire BD, Weiner JH. Molecular biology, biochemistry and bioenergetics of fumarate reductase, a complex membrane-bound iron-sulfur flavoenzyme of *Escherichia coli*. Biochim Biophys Acta 1985;811: 381–403.
[12] Heinz M. Encyclopedic reference of parasitology. 2nd ed. Berlin: Springer; 2001.
[13] Islam MK, Miyoshi T, Yamada M, Alim MA, Huang X, Motobu M, et al. Effect of piperazine (diethylenediamine) on the moulying proteome express and pyrophosphate activity of *Ascaris suum* lung-stage larvae. Acta Trop 2006;99:208–17.
[14] Miyazaki I. Helminthic zoonoses. Tokyo: International Medical Foundation of Japan; 1991. p. 295–305.
[15] Takamiya S, Furushima R, Oya H. Electron transfer complexes of *Ascaris suum* muscle mitochondria I. Characterization of NADH-cytochrome *c* reductase (complex I–III), with special reference to cytochrome localization. Mol Biochem Parasitol 1984;13: 121–34.
[16] Lowry OH, Rosebrough NJ, Farr AL, Randall RJ. Protein measurement with the folin phenol reagent. J Biol Chem 1951;193:265–75.
[17] Miyadera H, Shiomi K, Ui H, Yamaguchi Y, Masuma R, Tomoda H, et al. Atopenins, potent and specific inhibitors of mitochondrial complex II (succinate–ubiquinone oxidoreductase). Proc Natl Acad Sci U S A 2003;100: 473–7.
[18] Tomitsuka E, Goto Y, Taniwaki M, Kita K. Direct evidence for expression of Type II flavoprotein subunit in human complex II (succinate–ubiquinone reductase). Biochem Biophys Res Commun 2003;311: 774–9.
[19] Kita K, Vibat CR, Meinhardt S, Guest JR, Gennis RB. One-step purification from *Escherichia coli* of complex II (succinate:ubiquinone oxidoreductase) associated with succinate-reducible cytochrome b_{556}. J Biol Chem 1989;264:2672–7.
[20] Miyadera H, Amino H, Hiraishi A, Taka H, Murayama K, Miyoshi H, et al. Altered quinone biosynthesis in the long-lived *clk-1* mutants of *Caenohabditis elegans*. J Biol Chem 2001;276:7713–6.
[21] Towbin H, Staehelin T, Gorton J. Electrophoretic transfer of proteins from polyacrylamide gels to nitrocellulose sheets: procedure and some applications. Proc Natl Acad Sci U S A 1979;76: 4350–4.
[22] Shägger H, Cramer WA, von Jagow G. Analysis of molecular mass and oligomeric states of protein complexes by blue native electrophoresis and isolation of membrane protein complexes by two-dimensional native electrophoresis. Anal Biochem 1994;217:220–30.
[23] Kho CW, Park SG; Lee DH, Cho S, Oh GT, Kang S, et al. Activity staining of glutathione peroxidase after two-dimensional gel electrophoresis. Mol Cell 2004;18:369–73.
[24] Geenen PL, Bresciani J, Boes J, Pedersen A, Eriksen L, Fagerholm HP, et al. The morphogenesis of *Ascaris suum* to the infective third-stage larvae within the egg. J Parasitol 1999;85:616–22.
[25] Jeska EL, Williams JF, Cox DF. *Ascaris suum*: larval returns in rabbits, Guinea pigs and mice after low-dose exposure to eggs. Exp Parasitol 1969;26: 187–92.
[26] Stormberg BE, Soulsby EJL. *Ascaris suum*: immunization with soluble antigens in the Guinea pig. Int J Parasitol 1977;7:287–91.
[27] Komuniecki PR, Vanover L. Biochemical changes during the aerobic–anaerobic transition in *Ascaris suum* larvae. Mol Biochem Parasitol 1987;22(2–3):241–8.
[28] Islam MK, Miyoshi T, Kasuga-Aoki H, Isobe T, Arakawa Y, Matsumoto Y, et al. Inorganic pyrophosphatase in the roundworm *Ascaris* and its role in the development and molting process of the larval stage parasites. Eur J Biochem 2003;270: 2814–26.
[29] Kita K, Shiomi K, Omura S. Advances in drug discovery and biochemical studies. Trends Parasitol 2007;23:223–9.
[30] Kuramochi T, Hirawake H, Kojima S, Takamiya S, Furushima R, Aoki T, et al. Sequence comparison between the flavoprotein subunit of the fumarate reductase (complex II) of the anaerobic parasitic nematode, *Ascaris suum* and the succinate dehydrogenase of the aerobic, free-living nematode, *Caenorhabditis elegans*. Mol Biochem Parasitol 1994;68: 177–87.
[31] Martini FH, Ober WC, Garrison CW, Welch K, Hutching RT. Fundamentals of anatomy and physiology. 4th ed. Upper Saddle River, New Jergy: Prentice Hall; 1998.
[32] Kita K, Takamiya S, Furushima R, Ma YC, Suzuki H, Ozawa T, et al. Electron-transfer complexes of *Ascaris suum* muscle mitochondria. III. Composition and fumarate reductase activity of complex II. Biochim Biophys Acta 1998;935: 130–40.
[33] Yamashita T, Ino T, Miyoshi H, Sakamoto K, Osanai A, Nakamaru-Ogiso E, et al. Rhodoquinone reaction site of mitochondrial complex I, in parasitic helminth, *Ascaris suum*. Biochim Biophys Acta 2004;1608: 97–103.

ANTIMICROBIAL AGENTS AND CHEMOTHERAPY, Jan. 2008, p. 164–170
0066-4804/08/$08.00+0 doi:10.1128/AAC.00378-07

Vol. 52, No. 1

Anaerobic NADH-Fumarate Reductase System Is Predominant in the Respiratory Chain of *Echinococcus multilocularis*, Providing a Novel Target for the Chemotherapy of Alveolar Echinococcosis▽

Jun Matsumoto,[1] Kimitoshi Sakamoto,[2]* Noriko Shinjyo,[2] Yasutoshi Kido,[2] Nao Yamamoto,[1] Kinpei Yagi,[3] Hideto Miyoshi,[4] Nariaki Nonaka,[1] Ken Katakura,[1] Kiyoshi Kita,[2] and Yuzaburo Oku[1]

Laboratory of Parasitology, Department of Disease Control, Graduate School of Veterinary Medicine, Hokkaido University, Sapporo, Japan[1]; Department of Biomedical Chemistry, Graduate School of Medicine, University of Tokyo, Tokyo, Japan[2]; Department of Medical Zoology, Hokkaido Institute of Public Health, Sapporo, Japan[3]; and Division of Applied Life Sciences, Graduate School of Agriculture, Kyoto University, Kyoto, Japan[4]

Received 20 March 2007/Returned for modification 21 June 2007/Accepted 10 October 2007

Alveolar echinococcosis, which is due to the massive growth of larval *Echinococcus multilocularis*, is a life-threatening parasitic zoonosis distributed widely across the northern hemisphere. Commercially available chemotherapeutic compounds have parasitostatic but not parasitocidal effects. Parasitic organisms use various energy metabolic pathways that differ greatly from those of their hosts and therefore could be promising targets for chemotherapy. The aim of this study was to characterize the mitochondrial respiratory chain of *E. multilocularis*, with the eventual goal of developing novel antiechinococcal compounds. Enzymatic analyses using enriched mitochondrial fractions from *E. multilocularis* protoscoleces revealed that the mitochondria exhibited NADH-fumarate reductase activity as the predominant enzyme activity, suggesting that the mitochondrial respiratory system of the parasite is highly adapted to anaerobic environments. High-performance liquid chromatography–mass spectrometry revealed that the primary quinone of the parasite mitochondria was rhodoquinone-10, which is commonly used as an electron mediator in anaerobic respiration by the NADH-fumarate reductase system of other eukaryotes. This also suggests that the mitochondria of *E. multilocularis* protoscoleces possess an anaerobic respiratory chain in which complex II of the parasite functions as a rhodoquinol-fumarate reductase. Furthermore, in vitro treatment assays using respiratory chain inhibitors against the NADH-quinone reductase activity of mitochondrial complex I demonstrated that they had a potent ability to kill protoscoleces. These results suggest that the mitochondrial respiratory chain of the parasite is a promising target for chemotherapy of alveolar echinococcosis.

Echinococcosis is a near-cosmopolitan zoonosis caused by helminthic parasites belonging to the genus *Echinococcus* (family Taeniidae) (18). The life cycle of *Echinococcus* spp. includes an egg-producing adult stage in the definitive hosts and a larval stage in intermediate hosts including humans. The larval stage of the parasite produces a large number of infective protoscoleces that develop to adult worms after being ingested by the definitive host, or they produce a new parasite mass when liberated inside the intermediate host, causing metastases of the parasite lesions. The two major species of medical and public health importance are *Echinococcus granulosus* and *E. multilocularis*, which cause cystic echinococcosis and alveolar echinococcosis (AE), respectively.

Human AE is a life-threatening disease, and without careful clinical management, it has a high fatality rate and poor prognosis. Humans acquire AE infection by ingesting eggs from adult parasitic worms. Early diagnosis and treatment (mainly by radical surgery) of human AE are difficult because the disease progresses slowly and usually takes more than several years before clinical symptoms become apparent. An efficient chemotherapeutic compound is still not available. The first choice for the chemotherapy of AE is benzimidazole derivatives (18), but they are parasitostatic rather than parasitocidal against larval *E. multilocularis*. Therefore, the development of highly effective antiechinococcal drugs is urgently needed.

Biological systems for energy metabolism are essential for the survival, continued growth, and reproduction of all living organisms. "Typical" mitochondria are usually considered to be oxygen-consuming, ATP-producing organelles. In fact, typical mitochondria, such as those found in mammalian cells, require oxygen to function. They use pyruvate dehydrogenase for oxidative decarboxylation of pyruvate to acetyl coenzyme A, which is then completely oxidized to CO_2 through the Krebs cycle. Most of the energy is produced by oxidative phosphorylation: the electrons from NADH and succinate are transferred to oxygen by the proton-pumping electron transfer respiratory chain in which ubiquinone (UQ) (Fig. 1A) is commonly used as an electron mediator. The backflow of the protons results in ATP formation by the mitochondrial ATP synthase.

In parasitic organisms, on the other hand, the carbohydrate and energy metabolic pathways of adult parasitic helminths differ greatly from those of their vertebrate hosts. The most important factors in this respect are the nutrient and oxygen supply (reviewed in references 4, 12, and 13). Parasitic hel-

* Corresponding author. Mailing address: Department of Biomedical Chemistry, Graduate School of Medicine, University of Tokyo, Tokyo 113-0033, Japan. Phone: 81 3 58418202. Fax: 81 3 58413444. E-mail: sakamok@m.u-tokyo.ac.jp.

▽ Published ahead of print on 22 October 2007.

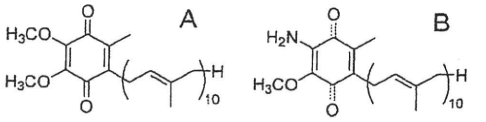

FIG. 1. Chemical structure of ubiquinone-10 (UQ_{10}) (E_m' = +110 mV) (A) and rhodoquinone-10 (RQ_{10}) (E_m' = −63 mV) (B).

minths have exploited a variety of energy-transducing systems during their adaptation to habitats in their hosts (7, 28). The parasitic nematode *Ascaris suum*, for example, resides in the host small intestine, where oxygen tensions are low, and exploits a unique anaerobic respiratory chain, called the NADH-fumarate reductase system, to adapt to its microaerobic habitat (Fig. 2) (2, 3, 14, 22; reviewed in reference 10). The NADH-fumarate reductase system is part of the unique respiratory system for parasitic helminthes and is the terminal step in the phosphoenolpyruvate carboxykinase-succinate pathway, which is found in many anaerobic organisms. Electrons from NADH are accepted by rhodoquinone (RQ) (Fig. 1B) via the NADH-RQ reductase activity of mitochondrial complex I and then transferred to fumarate through the rhodoquinol-fumarate reductase activity of mitochondrial complex II. The anaerobic electron transfer in complex I couples with proton transport across the mitochondrial inner membrane, providing ATP even in the absence of oxygen. This system, which does not normally function in mammalian mitochondria, is considered to be a good target for the development of novel anthelminthics (8, 9, 21). With regard to *Echinococcus* spp., the presence of both aerobic and anaerobic respiratory systems was previously suggested by a series of intensive studies (1, 16, 17), although the respiratory systems in this group of parasites are to be characterized in more detail.

In the present study, we prepared an enriched mitochondrial fraction from *E. multilocularis* protoscoleces and characterized the specific enzyme activities involved in mitochondrial energy metabolism as well as the quinone profile in the parasite's respiratory chain. Furthermore, based on findings reported previously by Yamashita et al. that quinazoline derivatives can inhibit the NADH-quinone reductase of mitochondria from *A. suum* (35), we tested several quinazoline-type compounds, with a view to developing novel antiechinococcal compounds.

MATERIALS AND METHODS

Isolation of *E. multilocularis* protoscoleces. We used the Nemuro strain of *E. multilocularis*, which is maintained at the Hokkaido Institute of Public Health (Sapporo, Japan). Mature larval parasites with protoscolex formation were obtained from cotton rats (*Sigmodon hispidus*) more than 4 months after oral infection with 50 parasite eggs. To isolate protoscoleces, the mature larval parasites were minced with scissors, pushed through a metal mesh, and washed repeatedly with physiological saline until host materials were thoroughly removed.

Preparation of enriched mitochondrial fractions. The enriched mitochondrial fractions of *E. multilocularis* protoscoleces were prepared essentially according to methods described previously for isolating adult *Ascaris* mitochondria (25, 26). Briefly, the isolated protoscolex sediment was suspended in 5 volumes of mitochondrial preparation buffer (210 mM mannitol, 10 mM sucrose, 1 mM disodium EDTA, and 50 mM Tris-HCl [pH 7.5]) supplemented with 10 mM sodium malonate. The parasite materials were homogenized with a motor-driven glass/glass homogenizer (six passes three to four times). The homogenate was diluted with the mitochondrial preparation buffer to 10 times the volume of the original protoscolex sediment and then centrifuged at 800 × *g* for 10 min to precipitate cell debris and nuclei. The supernatant was then centrifuged at 8,000 × *g* for 10 min to obtain the mitochondrial pellet. The pellet was resuspended in mitochondrial preparation buffer (without malonate) and centrifuged at 12,000 × *g* for 10 min. The resulting enriched mitochondrial fraction was suspended in mitochondrial preparation buffer (without malonate). The protein concentration was determined according to the method of Lowry et al. by using bovine serum albumin as a standard (15).

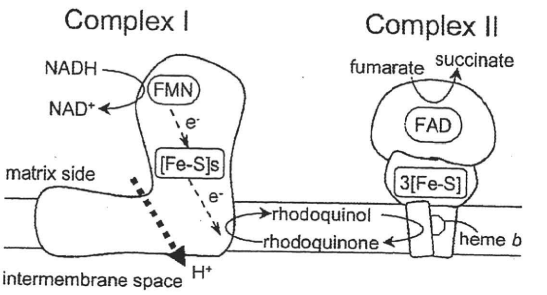

FIG. 2. Schematic representation of the NADH-fumarate reductase system in adult *A. suum*, which catalyzes the final step of the phosphoenolpyruvate carboxykinase-succinate pathway. In this system, the reducing equivalent of NADH is transferred to the low-potential RQ by the NADH-RQ reductase activity of mitochondrial complex I. This pathway ends with the production of succinate by the rhodoquinol-fumarate reductase activity of complex II. Electron transfer from NADH to fumarate is coupled to the site I phosphorylation of complex I via the generation of a proton-motive force. FMN, flavin mononucleotide; FAD, flavin adenine dinucleotide; [Fe-S]s and 3[Fe-S], iron-sulfur clusters.

Western blotting. An enriched mitochondrial fraction prepared from *E. multilocularis* protoscoleces and that from the liver of a cotton rat (used as the host animal for the parasite) were analyzed by Western blotting. Reactions were performed according to a method described previously by Towbin et al. (30). The proteins were separated by sodium dodecyl sulfate-polyacrylamide gel electrophoresis on a 10% or 15% acrylamide gel and electrophoretically transferred onto a nitrocellulose membrane. The membrane was soaked in 1:5,000 anti-cytochrome *c* oxidase subunit IV antibody (component of the ApoAlert cell fractionation kit; Clontech Laboratories) in phosphate-buffered saline containing 0.05% (wt/vol) Tween 20 and 2% (wt/vol) skim milk. The membrane was incubated for 60 min at room temperature and then washed three times for 10 min with washing buffer, which consisted of 0.05% (wt/vol) Tween 20 in phosphate-buffered saline. Alkaline phosphatase-conjugated goat anti-mouse immunoglobulin G was then added as a secondary antibody, and the mixture was incubated for 30 min. After another wash with washing buffer, the membrane was soaked in reaction buffer (100 mM Tris-HCl [pH 9.5], 100 mM NaCl, 5 mM $MgCl_2$, 500 μg/ml of 4-nitroblue tetrazolium chloride, and 165 μg/ml of 5-bromo-4-chloro-3-indolylphosphate) to initiate the development of a colored product. Finally, the membrane was washed with distilled water to stop the reaction. For Western blotting, the amounts of parasite and cotton rat mitochondrial samples were normalized by the total protein amount or cytochrome *c* oxidase activity (see below).

Enzyme assays. All enzyme assays using the enriched mitochondrial fractions were performed in a 0.7- or 1-ml reaction mixture at 25°C. The reagents used in each assay were mixed with reaction buffer containing 30 mM potassium phosphate (pH 7.4) and 1 mM $MgCl_2$. The final mitochondrial protein concentration was 80 μg per ml of reaction mixture. For all reactions performed under anaerobic conditions, the reaction medium was supplemented with 100 μg/ml glucose oxidase, 2 μg/ml catalase, and 10 mM β-D-glucose and left for 3 min to achieve anaerobiosis. NADH oxidase activity in the isolated mitochondrial fraction was determined in the presence or absence of 2 mM KCN, 100 mM malonate, or both by measuring the absorbance of NADH at 340 nm (ε = 6.2 mM^{-1} cm^{-1}). The reaction was initiated by the addition of 100 μM of NADH to the mixture. Succinate dehydrogenase (SDH) activity was determined by monitoring the absorbance change of 2-(4,5-dimethyl-2-thiazolyl)-3,5-diphenyl-2*H*-tetrazolium bromide (MTT; 60 μg/ml) at 570 nm in the presence of 120 μg/ml phenazine methosulfate and 2 mM KCN. The reaction was initiated by the addition 10 mM of succinate to the mixture. Succinate-quinone reductase activity was assayed under aerobic or anaerobic conditions in the presence of 0.1%(wt/vol) sucrose monolaurate by determining the amount of decyl UQ (dUQ) or decyl RQ (dRQ)

from the absorbance change at 278 nm (ε = 12.7 mM^{-1} cm^{-1}) or 287 nm (ε = 9.2 mM^{-1} cm^{-1}), respectively. Decyl rhodoquinol-fumarate reductase activity was measured under anaerobic conditions in a reaction mixture containing 0.1% (wt/vol) sucrose monolaurate. In this reaction, 60 μM dRQ was reduced to decyl rhodoquinol in the cuvette by adding 200 μM $NaBH_4$. The reaction was started by adding 5 mM fumarate to the mixture, and the oxidation of decyl rhodoquinol was monitored at 287 nm. NADH-fumarate reductase activity was determined by monitoring the oxidation of NADH (100 μM) at 340 nm under anaerobic conditions. The reaction was initiated by the addition of 5 mM fumarate as an electron acceptor. NADH-quinone reductase activity assays were carried out under anaerobic conditions using the same reaction mixture as that used for the NADH-fumarate reductase activity assay except that 60 μM dUQ or dRQ was used as an electron acceptor instead of fumarate. The enzyme activity was determined by monitoring the absorbance change of NADH at 340 nm. Ubiquinol oxidase activity was determined by monitoring the absorbance change of ubiquinol-1 (150 μM) at 278 nm (ε = 12.7 mM^{-1} cm^{-1}) in the presence or absence of 2 mM KCN. The activity of cytochrome *c* oxidase was determined as *N,N,N',N'*-tetramethyl-*p*-phenylenediamine dihydrochloride (TMPD) oxidase activity, which was measured by monitoring the absorbance change of TMPD (500 μM) at 610 nm (ε = 11.0 mM^{-1} cm^{-1}) in the presence or absence of 2 mM KCN.

Enzyme inhibition assays. Based on the findings of Yamashita et al. showing that that quinazoline-type compounds inhibit the NADH-quinone reductase activity of *A. suum* complex I (35), we determined 50% inhibitory concentration (IC_{50}) values of the quionazoline-type compounds against NADH-fumarate reductase activity of the parasite mitochondria and the NADH oxidase activity of bovine heart mitochondria (see "Enzyme assays"). The compounds used in the assays included quinazoline and its derivatives 6-NH_2, 6-$NHCO(CH{=}CH_2)$, 7-NH_2, 8-OH, 8-OCH_3, 8-OCH_2CH_3, and 8-$OCH(CH_3)_2$.

Analysis of the quinone profile of isolated mitochondria. Quinones were extracted from lyophilized mitochondria essentially according to a method described previously by Takada et al. (24). A lyophilized mitochondrial sample (2.9 mg protein) was crushed into powder before extraction, vortexed in 2:5 (vol/vol) ethanol/*n*-hexane for 10 min, and centrifuged at 20,000 × *g* for 5 min at room temperature. The supernatants were pooled, and the extraction of quinones was repeated twice. Pooled extracts were evaporated to dryness, dissolved in ethanol, and kept in the dark until high-performance liquid chromatography (HPLC) analysis. Quinones were applied to a reverse-phase HPLC column (Inertsil ODS-3 [5 μm and 4.6 by 250 mm]; GL Science) and eluted under isocratic conditions (1 ml/min) with 1:4 (vol/vol) diisopropyl ether-methanol at 25°C. The molecular species of the eluted quinones were identified by their retention times and by their spectral characteristics as measured with a UV-visible photodiode array (Shimadzu SPD-10-A). The concentration of quinones was determined spectrophotometrically. The major quinone detected was confirmed by mass spectrometry (MS) using an Applied Biosystems API-165 LC/MS system with electrospray ionization.

In vitro treatment of *E. multilocularis* protoscoleces. *E. multilocularis* protoscoleces were obtained as described above (see "Isolation of *E. multilocularis* protoscoleces"). The parasite materials were placed into culture medium suitable for the long-term maintenance of the protoscoleces in vitro (27). The parasite cultures were kept in a six-well plate at a density of approximately 500 protoscoleces per ml of culture medium, and half of the medium was replaced twice a week. This culture condition was also applied during in vitro treatment of the parasite. To examine the efficacy of chemical compounds against living *E. multilocularis* protoscoleces, the parasites were kept in the culture medium supplemented with 5 or 50 μM of each compound, including quinazoline and its 8-OH derivative, rotenone (a specific inhibitor of mitochondrial complex I) (19) and nitazoxanide (a compound with strong protoscolicidal action) (32). One control group was supplemented with 0.5% (vol/vol) dimethyl sulfoxide (vehicle) alone, and all conditions were assayed in triplicate. The viability of protoscoleces was determined by microscopic analysis of more than 170 protoscoleces per well for motile behavior and the ability to exclude trypan blue (32).

RESULTS

Preparation of enriched mitochondrial fractions. To characterize the mitochondrial respiratory chain of *E. multilocularis* protoscoleces, we prepared enriched mitochondrial fractions from the parasite. Approximately 80 g of larval *E. multilocularis* (containing approximately 10^5 protoscoleces per gram) was obtained from each cotton rat more than 4 months after oral infection with 50 parasite eggs. Approximately 20 g of the larval parasite was used per isolation of protoscoleces, yielding 2 ml of cleaned protoscolex sediment (Fig. 3). The enriched mitochondrial fractions were prepared from the protoscolex sediment as described in Materials and Methods. Each 1 ml of protoscolex sediment (containing 4.5 × 10^5 protoscoleces) yielded approximately 4 mg of mitochondria. Western blotting using an antibody to mammalian cytochrome *c* oxidase detected a specific band in the mitochondria from the liver of a cotton rat but not in mitochondria from *E. multilocularis* protoscoleces even when the amounts of both mitochondrial samples were normalized according to cytochrome *c* oxidase activity (data not shown). These results demonstrated that the enriched mitochondrial fractions from the parasite were sufficiently free of host components for use in enzyme assays and quinone analyses. In order to assess the quality of mitochondria, intactness was examined by the reactivity of NADH, which is a non-membrane-permeable substrate. NADH oxidase activity was not detected in the isotonic buffer, whereas it was fully activated in hypotonic buffer after a freeze-thaw treatment of the enriched mitochondrial fraction. Based on the results obtained, the method applied here for mitochondrial preparation seemed to be appropriate.

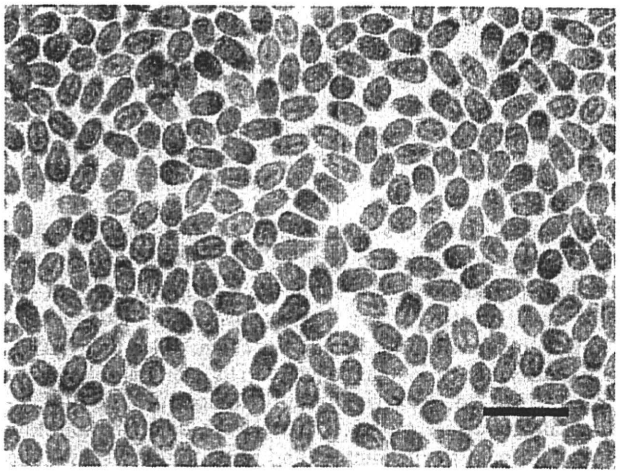

FIG. 3. Protoscoleces of *E. multilocularis* (Nemuro strain) used for the preparation of enriched mitochondrial fractions of the parasite and subsequent analyses. Bar, 500 μm.

Enzyme activities of *E. multilocularis* mitochondria. The specific enzyme activities involved in the mitochondrial respiratory chain of *E. multilocularis* protoscoleces are shown in Table 1. Parasite complex II exhibited an SDH activity of 103 nmol/min/mg. The specific activity of succinate-dUQ reductase was comparable to that of SDH activity (98.9 nmol/min/mg), whereas the succinate-dRQ reductase activity was lower (16.6 nmol/min/mg). The specific activity of decyl rhodoquinol-fumarate reductase, which is the reverse reaction of the succinate-RQ reductase activity of complex II, was determined to be 60.2 nmol/min/mg. The mitochondria of *E. multilocularis* protoscoleces exhibited NADH oxidase activity of 9.1 nmol/min/mg, which was almost eliminated by 2 mM KCN and 100 mM malonate. Ubiquinol-1 oxidase and TMPD oxidase activities were determined to be 4.4 nmol/min/mg and 12.6 nmol/

TABLE 1. Specific activities of mitochondrial respiratory enzymes in *E. multilocularis* protoscoleces

Assay	Sp act[a] (nmol/min/mg of protein) (mean ± SD)
SDH	103 ± 16
Succinate-quinone reductase	
dUQ (anaerobic)	98.9 ± 12
dRQ (anaerobic)	16.6 ± 3.5
Quinol-fumarate reductase (decyl rhodoquinol) (anaerobic)	60.2 ± 18
NADH oxidase	9.1 ± 2.1
NADH oxidase with:	
2 mM KCN	7.3 ± 1.5
100 mM malonate	4.4 ± 0.4
2 mM KCN and 100 mM malonate	1.7 ± 0.7
Ubiquinol-1 oxidase	4.4 ± 0.6
TMPD oxidase	12.6 ± 6.3
NADH-fumarate reductase (anaerobic)	45.0 ± 8.1
NADH-quinone reductase	
dUQ (anaerobic)	32.1 ± 2.7
dRQ (anaerobic)	61.3 ± 4.3

[a] Specific activities were obtained from at least three independently isolated mitochondria.

min/mg, respectively. These activities were completely inhibited by 2 mM KCN. Under anaerobic conditions, the specific activity of NADH-fumarate reductase was 45 nmol/min/mg, which was much higher than the NADH oxidase activity. The specific activity of NADH-dUQ reductase and NADH-dRQ reductase of complex I were determined to be 32.1 and 61.3 nmol/min/mg, respectively.

Quinone components in *E. multilocularis* mitochondria. To determine which quinones act as physiological electron mediators in the mitochondrial respiratory system of *E. multilocularis* protoscoleces, HPLC analyses were performed. As shown in Fig. 4A, the enriched mitochondrial fractions contained only one major quinone component at a retention time (*Rt*) of 22.4 min. The peak fraction exhibited a characteristic absorption maximum for RQs at 283 nm (Fig. 4B) (20). Subsequent MS analysis confirmed that the primary quinone of the parasite was RQ_{10} (electrospray ionization-MS *m/z* 848.8 $[M + H]^+$). The concentration of RQ_{10} was determined to be 0.73 nmol/mg of mitochondrial protein.

Effects of inhibitors on NADH-fumarate reductase in *E. multilocularis* mitochondria. To investigate the inhibitory effect of quinazoline (Fig. 5A) and its derivatives on the enzymatic activities in the anaerobic respiratory system of *E. multilocularis* mitochondria, we determined IC_{50} values against the NADH-fumarate reductase activity of the enriched mitochondrial fraction of the parasite. We found that all of the compounds inhibited the NADH-fumarate reductase activity of the parasite to some extent. Quinazoline and its derivatives including 6-NH_2, 6-NHCO($CH{=}CH_2$), 7-NH_2, 8-OH, 8-OCH_3, 8-OCH_2CH_3, and 8-$OCH(CH_3)_2$ exhibited IC_{50} values of 2.3, 2.1, 16, 62, 71, 48, 4,100, and 910 nM, respectively. Of the compounds tested, the 8-OH derivative (Fig. 5B) exhibited relatively selective inhibition against the NADH-fumarate reductase activity of *E. multilocularis* protoscoleces compared with the NADH oxidase activities of mammalian mitochondria: the IC_{50} values of quinazoline and its 8-OH derivative for

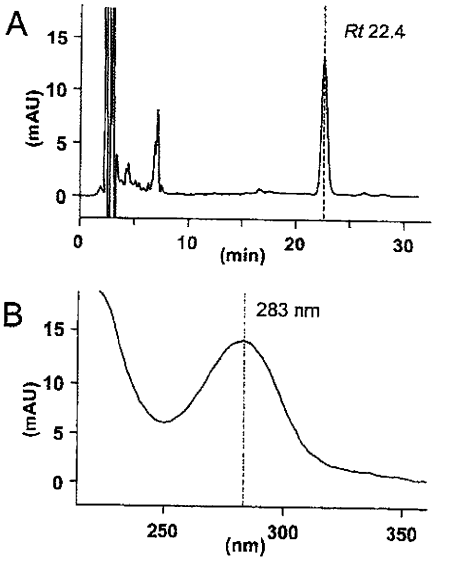

FIG. 4. (A) HPLC analysis of quinones extracted from the enriched mitochondrial fraction of *E. multilocularis* protoscoleces. Detailed experimental conditions are described in Materials and Methods. The highest peak had a retention time of 22.4 min (arrow). (B) Absorption of this peak was 283 nm, suggesting that it contained an RQ. mAU, milli-absorbance units.

the NADH oxidase activities of mammalian (bovine heart) mitochondria were 0.40 and 230 nM, respectively.

Effects of inhibitors on living *E. multilocularis* protoscoleces. In order to examine the parasite-killing activities of the quinazoline-type compounds with different degrees of inhibitory effects against NADH-fumarate activities of *E. multilocularis* protoscoleces, we performed in vitro treatment of the parasite using quinazoline and its 8-OH derivative. The viability of the *E. multilocularis* protoscolex was progressively reduced during in vitro treatment of the parasites with 50 μM of the 8-OH derivative, and by day 5, all the parasites died (Fig. 6). The same compound did not have an obvious antiparasitic effect when used at a concentration of 5 μM. On the other hand, nonsubstituted quinazoline, which showed lower IC_{50} values with the enzymatic assay, eliminated the parasites on days 5 and 7 of in vitro treatment when used at 50 and 5 μM, respectively. Treatment with rotenone, a specific inhibitor of mitochondrial complex I (19), affected the viability of the parasite in a manner similar to that of the 8-OH derivative. The anti-echinococcal effect of nitazoxanide was relatively mild: even in

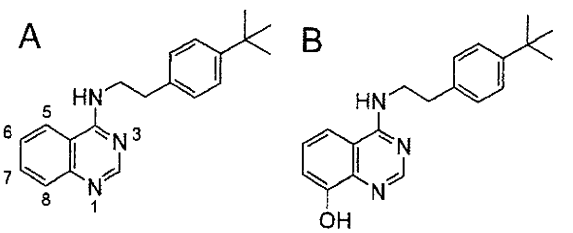

FIG. 5. Structures of quinazoline (A) and its 8-OH derivative (B) used for the enzyme inhibition assays and in vitro treatment of *E. multilocularis* protoscoleces.

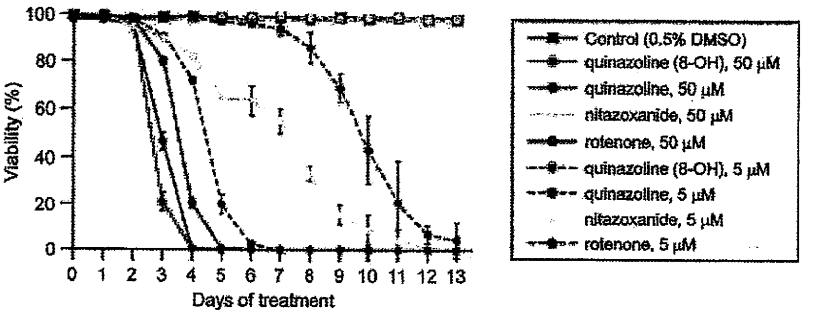

FIG. 6. Viability of *E. multilocularis* protoscoleces during in vitro treatment with quinazoline and its 8-OH derivatives, rotenone and nitazoxanide. Each compound was added to the culture medium at 5 or 50 μM. The results represent the means ± standard deviations of at least triplicate samples. DMSO, dimethyl sulfoxide.

the presence of 50 μM nitazoxanide, the viability decreased, but it did so only gradually, and it took 13 days before all the protoscoleces died. This compound did not affect parasite viability when used at 5 μM.

DISCUSSION

The most notable finding of the present study is that *E. multilocularis* protoscoleces possess a unique mitochondrial respiratory system that is highly adapted to anaerobic conditions. Specifically, the predominant enzymatic activity in the enriched mitochondrial fraction prepared from the parasite protoscoleces is the NADH-fumarate reductase system, which does not normally function in the aerobic respiratory chain of mammals. Thus, we infer that mitochondrial respiratory system of *E. multilocularis* would be a good target for the development of novel selective antiechinococcal compounds as demonstrated previously for other helminthic diseases (8, 21).

As early as 1957, Agosin found that *E. granulosus* protoscoleces have both aerobic and anaerobic respiratory systems and that glycolytic inhibitors are effective against both of them, indicating that they both depend on glycolysis (1). Subsequently, McManus and Smyth observed that protoscoleces cultured under anaerobic conditions produce more succinate than parasites kept under aerobic conditions, suggesting that the parasites survive under anaerobic conditions by utilizing the NADH-fumarate reductase system (16). Furthermore, McManus and Smyth reported that the specific activity of fumarate reductase in *Echinococcus* protoscoleces is lower than those of enzymes involved in the tricarboxylic acid cycle (17). These results, however, did not establish the importance of NADH-fumarate reductase activity in the mitochondrial respiratory system of the parasite because the other enzyme activities were not analyzed.

In the present study, we focused on the enzyme activities of the mitochondrial respiratory system of the parasite to determine whether the system is adapted to anaerobic conditions. Using the enriched mitochondrial fractions prepared from *E. multilocularis* protoscoleces, we showed that the activity of NADH-fumarate reductase in the respiratory system of the parasite is predominant compared with that of NADH oxidase, an enzyme involved in aerobic respiration in aerobic organisms such as mammals. Furthermore, direct measurements of complex II activities in both directions (i.e., succinate-RQ reductase and rhodoquinol-fumarate reductase activities) indicated that parasite complex II functions more favorably as a rhodoquinol-fumarate reductase in the presence of RQ/rhodoquinol. Thus, our results using isolated mitochondria of *E. multilocularis* protoscoleces coupled with assay systems for the determination of the parasite's enzyme activities revealed for the first time that the parasite mitochondria are highly adapted to anaerobic environments.

Analyses of the quinone components of *E. multilocularis* mitochondria revealed that RQ_{10} (Fig. 1B), whose redox potential is much more negative (E_m' [midpoint potential] = −63 mV) than that of UQ_{10} (E_m' = +110 mV) (Fig. 1A), was the primary quinone component of parasite mitochondria. In other parasitic helminths, like *A. suum* and *Hymenolepis diminuta*, RQ is an essential component of the NADH-fumarate reductase system (5, 11). In addition, van Hellemond et al. previously demonstrated that for all eukaryotes, the relative amount of RQ compared to the total amount of quinones correlates well with the importance of fumarate reduction in vivo (31). Similarly, during the development of the liver fluke *Fasciola hepatica*, there is a good correlation between the quinone composition and the importance of fumarate reduction in vivo (31). Therefore, RQ seems to be an essential component of fumarate reduction in eukaryotic respiration. Although menaquinone-related fumarate reduction in prokaryotes is well known (33, 34), there is no evidence that menaquinone serves this function in eukaryotes. In this study, enzyme assays demonstrated that the mitochondria from *E. multilocularis* possess NADH-fumarate activity as the predominant activity. In addition, the NADH-dRQ reductase activity was much higher than that of NADH-dUQ reductase, indicating that *E. multilocularis* complex I may interact preferentially with RQ rather than with UQ. Taken together, these results indicate that, as in other metazoan eukaryotes with anaerobic respiratory systems, *E. multilocularis* protoscoleces have a unique respiratory system that is highly adapted to anaerobic environments and in which RQ_{10} is used as the primary electron mediator.

Spiliotis et al. recently reported that the in vitro growth of larval *E. multilocularis* is more active under anaerobic than aerobic conditions (23). Thus, our findings for the respiratory system of *E. multilocularis* protoscoleces are consistent with the observations reported previously by Spiliotis et al. Larval *E. multilocularis* containing a large number of protoscoleces